Computational Investigation of Magnetic Interactions: Combining First Principles and Model Approaches

by

Michelle D. Johannes
B.A. (Mt. Holyoke College) 1993
M.S. (UC Davis) 1998

DISSERTATION

Submitted in partial satisfaction of the requirements for the degree of

DOCTOR OF PHILOSOPHY

in

Physics

in the

OFFICE OF GRADUATE STUDIES

of the

UNIVERSITY OF CALIFORNIA, DAVIS

Approved:

Chair Warren E. Pickett, Professor of Physics	Date
Richard T. Scalettar, Professor of Physics	Date
Rajiv R. P. Singh, Professor of Physics	Date

Committee in charge
2003

Michelle D. Johannes
September 2003
Physics

Computational Investigation of Magnetic Interactions: Combining First Principles and Model Approaches

Abstract

Magnetic materials have traditionally been separated into two categories: localized and delocalized (or itinerant) systems. The study of itinerant magnetic materials with first principles approaches has been very successful, while model calculations have been the favorite for localized systems. This work is an attempt to use both methodologies in combination to study the magnetic properties of three systems with varying levels of localization.

$MgCNi_3$ is a superconductor that may be near a ferromagnetic instability, raising the intriguing possibility of a transition to a state in which the two behaviors exist simultaneously. $CaCu_3Ti_4O_{12}$ is an antiferromagnetic insulator with a very simple magnetic order which cannot be explained by the standard superexchange picture unless interactions between spins separated by more than a lattice constant exist. EuN is a compound with strong spin and orbital moments which are equal in magnitude and cancel one another. Calculations show that this 'non-magnetic' state actually has an underlying order in which all spin moments are aligned with each other and anti-aligned with all orbital moments.

Density functional based methods are used to calculate accurate ground state properties, and the resulting information is used in conjunction with a model system appropriate to each case in order to gain accurate and intuitive information about the intrinsic magnetic interactions in each system.

To my parents,

Wayne and Jeanne

Contents

List of Figures

List of Tables

Acknowledgments

Many people have contributed toward the completion of this thesis, but none more substantially than my advisor. Simultaneously astonishingly productive and open to sharing his time, he has increased both my knowledge of and my enthusiasm for physics. Warren, thank you for your endless patience, your valuable suggestions, the opportunities you have provided for me, your insight, and especially for always taking me seriously while I was learning. Thank you also for creating and encouraging a collaborative and enjoyable working group. I couldn't have asked for a better mentor and role model.

My research group has also been an integral part of my work. Group meetings and impromptu gatherings in the hall have consistently proved invaluable learning experiences. Thank you, Alan, Deepa, Helge, Jan, Joon, Kris, Kwan-Woo, Meichan, Wei, and Sasha for all the discussions, explanations and arguments. Learning along with all of you has been truly enjoyable. Thank you, Deepa and Wei, for adding that special element so often missing from research groups, 'thanks' to Kris for reminding me of what I don't know, and a special thanks to Helge for the daily coffee discussions during which I learned enormous amounts about physics and life in general. I will very much miss working with all of you on a daily basis.

Finally, I would like to thank my friends and family for their support and encouragement. Thank you Mani, Pete, and Kristi for all the good times and great company. Patrick, thank you for food, encouragement and friendship. Mom and Dad, obviously without you, I wouldn't be here - in so many ways.

head9

Chapter 1

Goals

The goal of this research is to combine accurate density functional methods with physically motivated models to investigate the microscopic mechanisms underlying observed (or predicted) behavior of three magnetic compounds. The basis for all studies is band structure information gained from density functional theory (DFT) computations. Band theory techniques are now well-refined, through years of application and study. DFT can provide accurate ground state information for many diverse systems, including those with magnetic order. The deficiencies incurred through the use of the local density approximation (LDA) have been extensively researched and a body of intuition about which calculated properties are likely to be accurate and which are not has been built up. Therefore, first principles calculations which rely on this formulation can be trusted to provide reliable information in a wide variety of systems and to err in ways that are understood and reasonably predictable. Nonetheless, the facts remain that 1) DFT is only formally valid for the ground state and 2) that error is introduced through the approximation to the exchange-correlation potential.

Systems in which electrons are strongly correlated are not well modeled using the LDA and excitation information is absent or hard to justify. The employment of model systems in conjunction with first principles calculations can in some circumstances supplement or improve theoretical results, bringing them into closer alignment with experimental data, the litmus test of legitimacy. Building on the foundation of DFT results, model calculations are performed for some aspect of each of the three compounds which are studied here.

The three compounds whose investigation comprises the body of this work were chosen because they represent a diverse group of d and f electron systems. In choosing these particular systems, aspects of many behaviors can be studied. As a group, these materials exhibit localized and itinerant magnetism; ferromagnetism and antiferromagnetism; d-like magnetic moments and f-like magnetic moments; and metallic and insulating behavior. Each compound contains the hallmark characteristics of the overall type it is meant to represent. Therefore methodologies and techniques developed or refined to deal with each type of compound are portable to other compounds of similar type or category.

The broad spectrum of behaviors observed in the chosen materials allows a variety of model techniques to be employed, with a number of different relationships to the first principles calculations which are used uniformly throughout this work. In the first compound, the use of the model saves computational time and effort and provides insight into the factors which might drive a magnetic transition. In the second case, the model is applied in order to give information about magnetic excitations which the specifically ground state information from DFT cannot provide. In the final case, ideas from model Hamiltonian calculations are incorporated directly into the first principles calculation, somewhat

blurring the line between the two. In every case, the emphasis is on using the two methodologies, first principles electronic structure and model systems, cooperatively rather than comparatively.

In addition to being broadly representative of a class, each compound was chosen because of its particular properties. The general program of combining first principles and model approaches is justified for these specific compounds not only for the general knowledge gained through the experience of applying different methodologies, but also because each exhibits significant and interesting behavior on its own.

The structure of this work is organized as follows: An introduction to the first principles methodologies which form the backbone of all studies contained here is given in chapter 2. In chapter 3, a very basic delineation between types of magnetism is drawn and a general description of the ability of DFT to deal with each type is reviewed. Chapter 4 provides a brief introduction to each magnetic system, how it fits into the wider picture of magnetism and why it individually merits study. The details of the computational work, interpretations, derivation of models and explicit results are contained in the separate chapters corresponding to each compound.

Chapter 2

Density Functional Theory and Techniques

Present day density functional theory (DFT) methods rest on an assumption known as the Born-Oppenheimer approximation. Since in an extended system, the electrons are extremely mobile compared to the ion cores, the latter are assumed to be immobile. This is not exactly true, even at the absolute zero of temperature, but corrections can be treated as, for example, electron-phonon interactions. The configuration of the electrons is assumed to be at all times in equilibrium with the potential generated by the ions. Therefore, the many body problem of atoms in a solid is reduced to the problem of determining the configuration of the electrons in the static potential of the ion cores.

Hohenberg and Kohn showed [1] that the fundamental variable of the ground state of an electronic system is the electron density. The energy of a many electron system can be expressed as a functional of this density. The minimum of the functional occurs at the

ground state density and provides the ground state energy of the system. Other ground state properties are also density functionals and are similarly minimized by the ground state density. These theorems are powerful because they eliminate the necessity of knowing the wave function, replacing it with the much simpler variable of density. Though the existence of the energy functional is formally proven and its inherent usefulness is obvious in the context of these theorems, there is little information about what exactly the form of the functional is.

Soon after, Kohn and Sham developed a workable scheme [2] for applying the density function formalism. First, the energy functional can be written without approximation (neglecting the ion-ion interaction) as:

$$E[\rho] = T[\rho] + E_H[\rho] + E_{ex}[\rho] + E_{corr}[\rho] + E_{ext}[\rho] \tag{2.1}$$

where T is the kinetic energy, E_H is the Hartree energy, E_{ex} the exchange term, E_{corr} is the correlation energy (correction to the approximation made by the Hartree term), and E_{ext} is the electron-ion interaction. Some of these terms have well-known forms, while others are not known at all. The kinetic energy as a functional of the density is not known and the correlation energy is by definition that which is not accounted for by the other terms. The exchange term is non-local and is known exactly in terms of the wavefunctions.

Kohn and Sham supposed that the density is written in terms of N single particle orbitals, where N is the number of electrons in the system:

$$\rho(\vec{r}) = \sum_{i=1}^{N} \psi_i^*(\vec{r})\psi_i(\vec{r}) \tag{2.2}$$

Finally, the kinetic energy functional is written as the kinetic energy of a non-interacting system with the same density as the interacting system, and the error introduced by this representation is grouped with the exchange and correlation operators into a single term, written as E_{xc}. E_{xc} groups the known exchange energy along with the unknown correlation energy and correction to single-particle kinetic energy in anticipation of the major approximation of DFT, the local density approximation. So far, no information has been lost, since terms have simply been shuffled around and defined. The functional can still be written without approximation as the sum of the single particle kinetic energy, the Hartree term, the exchange-correlation term (which contains the non-single particle kinetic energy) and the electron-ion term:

$$E[\rho] = T_s[\rho] + E_H[\rho] + E_{xc}[\rho] + E_{ext}[\rho] \tag{2.3}$$

2.1 Local Density Approximation

The exchange-correlation energy is a functional of the density, but is not known analytically. It can be written exactly as $\int \rho(\vec{r})\epsilon_{xc}(\vec{r};\rho)d\vec{r}$, but $\epsilon_{xc}(\vec{r};\rho)$ is non-local *i.e.* it depends on the density everywhere, and as such is unmanageable. Long before DFT emerged, Slater [3] suggested the use of the local density approximation (LDA). However, it came into wide use when combined with the Kohn-Sham formulation of DFT, as an approximation to the true exchange correlation energy. The LDA assumes that the exchange correlation energy can be written as:

$$E_{xc}[\rho] = \int \rho(\vec{r})\epsilon_{xc}(\rho(\vec{r}))d\vec{r} \tag{2.4}$$

Now ϵ_{xc} is a simple, local function of the density, not a functional. The specific value of the function is taken from that of the homogeneous electron gas. In the homogeneous electron gas, the exchange-correlation energy is truly a local function of the density because the density is the same everywhere. Even this highly simplified case cannot be solved analytically and must be solved through numerical techniques. Several parameterizations of $\epsilon_{xc}(\rho)$ are available and commonly used.

The exchange correlation potential in the LDA is derived as:

$$v_{xc}(\vec{r}) = \frac{\delta E_{xc}[\rho]}{\delta\rho(\vec{r})} = \left[\frac{d}{d\rho}\{\rho\epsilon_{xc}(\rho)\}\right]_{\rho=\rho(\vec{r})} \tag{2.5}$$

The LDA can be pictured as taking the full, inhomogeneous system and dividing it into small boxes which are assumed to be approximately homogeneous. In each box, the density is calculated and the exchange correlation potential of a homogeneous electron gas at that specific density is used for the wider calculation.

The LDA is effective for systems in which the actual density varies slowly. In the limit that the density varies not at all, the real system and the homogeneous electron gas become identical and the LDA no longer constitutes an approximation. In practice, this means that systems which are strongly hybridized such that electron states are broad suffer the least error from the LDA, while localized systems will be treated less accurately.

2.1.1 Self-Consistent Formulation

Once the LDA has been implemented, the functional derivative of the energy with respect to the density can be taken:

$$\frac{\delta E}{\delta \rho} = \frac{\delta T_S[\rho]}{\delta \rho} + v_H(\vec{r}) + v_{xc}(\vec{r}) + v_{ext}(\vec{r}) = 0 \tag{2.6}$$

With the kinetic energy operator in its single particle form, $-\frac{\nabla_i^2}{2m}$, and the identification $v_{eff} = v_H + v_{xc} + v_{ext}$, this equation is identical to that of a non-interacting electron system moving in an external effective potential. Therefore it can be cast into a single particle Schrodinger-like equation, known as the Kohn-Sham equation, the solutions to which are the wave functions:

$$\left\{ -\frac{\nabla^2}{2m} + v_{eff}(\vec{r}) \right\} \psi_i(\vec{r}) = \epsilon_i \psi_i(\vec{r}) \tag{2.7}$$

The effective potential is a functional of the density so this equation must be solved self-consistently. The recipe for solving the self-consistent equations is:

1) Guess an initial density, $\rho_{in}(\vec{r})$

2) Formulate $v_{eff}[\rho_{in}(\vec{r})]$

3) Solve the Kohn-Sham equations to get $\{\psi(\vec{r})\}$ (2.8)

4) Calculate $\rho_{out}(\vec{r})$ from $\{\psi_i(\vec{r})\}$ according to Eq. 2.2

If $\rho_{out}(\vec{r})$ and $\rho_{in}(\vec{r})$ are sufficiently close $\longrightarrow$ END; *else*

5) Mix $\rho_{out}(\vec{r})$ and $\rho_{in}(\vec{r})$ to create a new $\rho_{in}(\vec{r})$; return to step 2

This process is repeated until the agreement between $\rho_{out}(\vec{r})$ and $\rho_{in}(\vec{r})$ meets some convergence criterion. Once the density is satisfactorily converged, the ground state energy can be calculated, along with any other desired ground state properties.

The LDA formulation of DFT can be extended to spin polarized systems in which there is a separate density for spin-up and spin-down: $\rho_{uparrow}(\vec{r}) + \rho_{downarrow}(\vec{r}) = \rho_{tot}(\vec{r})$. The equations and methods developed in this section remain the same, but separate potentials are used for each spin direction and a spin-polarized homogeneous electron gas must be used to obtain an expression for the exchange correlation potential. The approximation to the true exchange-correlation energy for a spin-polarized system is known as the LSDA (S for spin), but the common acronym LDA will be employed throughout this manuscript, whether the system is spin polarized or not.

2.2 Basis Sets

The basis set in which the Kohn-Sham eigenfunctions are expanded is an important choice which affects the accuracy of the calculation and the size of the matrix which will eventually have to be diagonalized. Two choices which represent different limits have traditionally been used: plane waves and atomic functions. The former will work well in regions where the states are free-electron-like, while the latter are a better choice to model the rapidly oscillating wave functions near the ion cores. The use of plane waves in computational schemes requires the application of a pseudo-potential without which the number of plane waves which must be retained is prohibitively large. Atomic functions, on the other hand, are ideal for reproducing the wave function of localized orbitals, but perform

poorly far away from ion centers where the real wave functions are decidedly plane wave-like. Transition metal systems are notoriously hard to treat with either of these methods because they exhibit both localized and delocalized behavior.

2.2.1 Linearized Augmented Plane waves (LAPW)

Slater first suggested a combination of these two basis sets known as Augmented Plane Waves (APW). In the APW method, two regions of every crystal system are identified. A spherical region (known as a muffin-tin sphere) with a radius R is drawn around each ion. The size of the sphere depends on the particular character of the ion and on the proximity of its nearest neighbors. Outside this radius, in the interstitial region, the eigenfunctions are expanded in plane waves.

$$\psi_{\vec{k}}(\vec{r})_{\text{interstitial}} = \frac{1}{V}\sum_{\vec{G}} e^{i(\vec{k}+\vec{G})\cdot\vec{r}} C_G \tag{2.9}$$

Inside the muffin tin spheres, solutions to an atomic-like Schrodinger equation are used.

$$\begin{gathered}\psi(\vec{r})_{\text{muffin-tin}} = \sum_{l,m} A_{lm} u_l(\vec{r}) Y_{lm}(\hat{r}) \\ \text{where} \quad u_l(\vec{r}) \quad \text{satisfies:} \\ \left[-\frac{d^2}{dr^2} + \frac{l(l+1)}{r^2} + V(r) - E_l\right] r u_l(r) = 0\end{gathered} \tag{2.10}$$

An APW is a plane wave in the interstitial matched continuously onto a set of atomic-like functions (the solutions of 2.10), such that there is no discontinuity in the

basis function at the boundary of the muffin-tin sphere. The plane wave is expanded onto a set of Y_{lm}'s and the coefficients are matched to those of the muffin-tin functions for the corresponding Y_{lm}. This matching determines the coefficient A_{lm}'s in terms of the plane wave coefficients, C_G. Though the basis function is continuous, there is a kink at the boundary of the muffin-tin sphere due to the difference in the slope of the plane wave and the atomic-like functions at the point of meeting. This results in a surface term in the kinetic energy (which depends on the spatial derivative of the wave function) that must be taken into account in the secular equation.

A main deficiency of the APW method is that there is a solution to the radial differential equation in Eq. 2.10 for every E_l, but not every E_l will produce a basis function that is equipped to model the real eigenfunction inside the sphere. Therefore, the E_l's must be found variationally in order to correctly yield the eigenstates and band energies. This results in a problem non-linear in the E_l's and adds considerable computational difficulty to any system for which APW's are used as a basis set.

Andersen proposed [4] adding the energy derivative of the radial function, $\dot{u}_l(r)$, to the existing function inside the muffin tin sphere. Each function would have its own coefficient, providing extra variational freedom inside the sphere such that the real eigenfunctions can be very accurately modeled. The errors introduced into the wave function by the energy parameter in this case are of order $(\epsilon - E_l)^2$. Errors in the band energy are even less significant, of order $(\epsilon - E_l)^4$. There are now two coefficients inside the sphere which must be determined. The first is determined in the standard way, by requiring that the basis function be continuous at the boundary. The remaining arbitrariness is removed by

requiring that the derivative also be continuous at the boundary. This final condition fully determines the coefficients and additionally removes the surface term in the kinetic energy, simplifying the secular equation.

The E_l's still pose one difficulty in many calculations. The basis orbitals of a given atom are generally divided into 'core' and 'valence' orbitals. The core orbitals are created using a strictly spherical potential and are required to go to zero at the muffin tin radius. Core functions are not APW's - they are atomic-like functions inside the sphere but have no contribution at all to the eigenfunction outside the sphere. The valence orbitals extend outside the muffin-tin radius and are always attached to a plane wave. The core and valence functions are orthogonal, provided the core state is completely confined within the sphere. There are states in some atoms which do not fall neatly into either category - these are known as 'semi-core' states. These states do not extend significantly beyond the sphere boundary, but are not fully confined either and are therefore not orthogonal to the APW valence states. This non-orthogonality can damage the accuracy of a calculation if, for a given l, the valence wave function has a non-trivial overlap with a semi-core state of the same l. A single linearization energy, E_l cannot possibly represent both the semi-core wave function and the valence wave function properly. More flexibility in the basis set is required if the energy spectrum is to be accurate. A simple technique to add this flexibility without significantly increasing computational effort is the local orbital extension. [5] With this technique, another basis function is added to those already inside the sphere. The new function is:

$$\psi_{lo}(r) = \left(A_{lm}u_l(E_l^{(1)}, r) + B_{lm}\dot{u}_l(E_l^{(1)}r) + C_{lm}u_l(E_l^{(2)}, r)\right) Y_{lm}(\hat{r}) \tag{2.11}$$

The first radial function and the energy derivative of that function are both evaluated using the original energy parameter, $E^{(1)}$, i.e. the parameter which best corresponds to the valence band energy. The final radial function is evaluated using a second energy parameter, with an energy more suitable to describing the semi-core state. The coefficients of the local orbital are set by requiring that the value of the function as well as its derivative go to zero at the sphere boundary. Normalization of the local orbitals renders the final coefficient arbitrary and it is therefore set to unity. Now sufficient flexibility is built into the basis set that core, semi-core and valence states can all be treated accurately.

2.3 APW+lo

Recently, an alternative to the LAPW basis set has been put forward [6] which allows for a smaller basis set overall, reducing computational time. The APW+lo basis set does not use the energy derivative of the radial function as part of the basis inside the sphere. As suggested by the name, the functions in the interstitial are still plane waves. The interior functions are of two types: the original APW's but with the E_l fixed (not varied) and a local orbital to correct for the fact that the APW alone does not have enough flexibility at a given E_l to adjust to the real band energy. In the APW+lo system, the wave function is expanded onto traditional APW's:

$$\psi(r) = \sum_{lm} A_{lm} u_l(E_l^{(1)}, r) Y_{lm}(\hat{r}) \qquad \text{Inside spheres} \tag{2.12}$$

$$\psi(r) = \sum_{\vec{G}} C_{\vec{G}} e^{i(\vec{k}+\vec{G})\cdot\vec{r}} \qquad \text{Interstitial}$$

In addition to the APW's, a local orbital is added for each l. In contrast to the local orbitals added to the LAPW basis functions, those of the APW+lo are evaluated at the *same* linearization energy as the APW:

$$\psi_{lo}(r) = [b_{lm} u_l(E_L^{(1)}, r) + c_{lm} \dot{u}_l(E_l^{(1)}, r)] Y_{lm}(\hat{r}) \tag{2.13}$$

The main advantage of the APW + lo method is that the boundary conditions at R are easier to fulfill. There is no need to match both the function and derivative inside and outside the sphere. The requirement that the function be continuous is sufficient to determine the APW coefficients and local orbital coefficients are determined by requiring that each go to zero at the boundary of the sphere. The basis functions are still linearized such that the exact choice of E_l will not affect the outcome of the calculations (provided E_l is reasonably chosen). The problem of semi-core states still exists and is treated by adding a second local orbital:

$$\psi_{lo}^{[2]}(r) = [b_{lm} u_l(E_L^{(1)}, r) + c_{lm} u_l(E_2^{(1)}, r)] Y_{lm}(\hat{r}) \tag{2.14}$$

Again, the function is forced to have zero value at the boundary and no condition is made on the derivative. Since a local orbital must be included with each APW, there will be more functions involved inside the spheres (compared to the LAPW basis set), which would enlarge the Hamiltonian matrix and increase the computational time. The increase,

however, is offset by a reduction in the required number of plane waves. Because the derivative isn't forced to be continuous, higher wavenumber plane waves are unnecessary and the cutoff can be set lower, reducing the overall computational time, especially for structures with large amounts of space between ions. The surface term in the kinetic energy re-enters the picture and must be accounted for. Though the kink in the basis functions does add a small measure of difficulty in writing the kinetic energy term, it has no overall effect on the resulting eigenfunctions which are smoothly continuous [6].

Both LAPW and APW+lo basis sets have been used in this research. There were no significant differences between results obtained from the two different methods in all cases where comparisons were done.

2.4 Fixed Spin Moment Procedure

The fixed spin moment (FSM) technique allows the total magnetic moment of the system to be fixed during the calculation. The magnetic moment per unit cell, given as $\int (\rho_{\uparrow}(\vec{r}) - \rho_{\downarrow}(\vec{r}))\, d\vec{r}$ is an input to the calculation. The energy functional is then minimized respecting this constraint. This allows the energy of a single system to be calculated at various magnetic moments.

In practice the FSM procedure involves computing separate Fermi energies for each spin channel. In the event that the chosen spin moment is the equilibrium spin moment, these two Fermi energies will be equal. This is equivalent to shifting the up and down occupations of the single particle energy levels by applying an external magnetic field, $H = \frac{\epsilon_{F\uparrow} - \epsilon_{F\downarrow}}{2\mu_B}$. To determine the total energy of an FSM calculation, each spin channel is filled to

the appropriate level and the energy of the field necessary to shift the occupations is added.

There are a number of reasons to apply the FSM procedure to a magnetic system. It is particularly important for systems with more than one local magnetic minima. In such cases the FSM procedure allows a mapping of these minima with respect to energy so that the various solutions can be studied. In some cases, a calculation may converge to a local minimum, rather than the correct global minimum. Constraining the calculation to converge to a value near the correct moment initially and then releasing the constraint allows the system to find its proper equilibrium. The FSM procedure can also be used to gain information about the energy vs. magnetic moment curve near the equilibrium which in turn gives the susceptibility.

2.5 LDA+U

The LDA gives reasonably accurate ground state results for systems in which the approximation to the exchange-correlation potential does not constitute a gross underestimation of electron-electron correlation. In strongly correlated systems, it can give results that are far from accurate and even unphysical. One attempt to correct for the deficiencies of the LDA is LDA+U, a method first suggested by Anisimov [7] *et al.* Recognizing the success of the Hubbard model in reproducing many qualitative aspects of strongly correlated systems, the LDA+U incorporates a Hubbard-like correction into the traditional self-consistent formulation of DFT. The aim is to exploit the strong points of both types of calculations, preserving the aspects of band theory that work well and including a corrective term from a model Hamiltonian to better account for strong correlation effects.

At a basic level, the idea of LDA+U is to add to the LDA formulation a Hubbard-type correlation energy, roughly of the form:

$$E = E_{LDA} + \frac{1}{2} \sum_{i\sigma \neq j\sigma'} U n_{i\sigma} n_{j\sigma'} \tag{2.15}$$

Here $n_{i\sigma}$ is the occupation of a local orbital i (spin σ) that must somehow be specified. Double counting terms have been neglected, but will be discussed in detail in a later section. The subscripts i and j label the individual orbitals of a given angular momentum quantum number, *i.e.* they run from 1 to 5 for d electrons and from 1 to 7 for f electrons. This correlation term accounts for interactions between specific orbitals and is a non-local functional of the density, in contrast to the mean-field correlation of the LDA. The on-site inter-orbital exchange term is also included, using the same non-local formulation. The orbital energies, ϵ_i, can be calculated based on the energy functional:

$$\frac{\partial E}{\partial n_i} = \epsilon_i = \epsilon_{LDA} + U(\frac{1}{2} - n_i) \tag{2.16}$$

Since n_i is the orbital occupation, the effect of adding the new term to the LDA formulation is to shift occupied orbitals down in energy and to shift unoccupied orbitals up in energy. This can fix one of the catastrophic failures of the LDA. In d and f electron systems with partially filled shells, the orbital energy levels are very nearly degenerate and therefore the mean-field treatment results in each orbital being partially filled, rather than some subset of orbitals being filled with the rest remaining empty. This erroneous partial filling of the orbitals gives a metallic ground state to compounds which are experimentally insulators, such as many transition metal oxides. The addition of the extra correlation term

yields the properly insulating ground state for these materials.

Identification of Orbitals

In order to add the new potential to the first principles scheme, the particular orbitals which are presumed to be strongly correlated must be separated out from the others. The method of separation, alas, depends on the basis set used in the calculation such that the LDA+U scheme is 'implementation dependent'. For local orbital basis sets such as LMTO, this process is relatively straightforward, whereas for LAPW or APW+lo, the process is less clear and not unique. The division of orbitals into strongly correlated and weakly correlated (requiring a correction and not) for these basis sets can be found explained clearly in the literature and will not be discussed in detail here. [8] Once this division is made, the result is a non-diagonal density matrix, $n^{\sigma}_{mm'}$, for each l selected to be strongly correlated. Each element, $n_{mm'}$ can be qualitatively thought of as the contribution to the density from the overlap of wave functions with lm and lm' character.

The U Energy Functional

Taking into account that the correlation between orbitals on a given site can depend on the shape of the orbitals, the Hubbard-like term in coordinate-system-independent (called 'rotationally invariant') form is written:

$$E^{U}[n] = \frac{1}{2} \sum_{\{m\},\sigma,\sigma'} n^{\sigma}_{mm'}(< m, m''|V_{ee}|m', m''' > \tag{2.17}$$

$$- < m, m''|V_{ee}|m''', m' > \delta_{\sigma,\sigma'})n^{\sigma'}_{m''m'''}$$

The final negative term is the inter-orbital exchange which is, specifically, the reduction of Coulomb energy associated with the alignment of spins. The matrix elements can be calculated if the Slater integrals, F_k are known:

$$< m, m''|V_{ee}|m', m''' > \; = \; \sum_k a_k(m, m', m'', m''')F_k \tag{2.18}$$

$$a_k(m, m', m'', m''') = \frac{4\pi}{2k+1} \sum_{q=-k}^{k} < lm|Y_{kq}|lm' >< lm''|Y_{kq}|lm''' >$$

The coefficients, a_k are calculated and the Slater integrals are obtained through the input of the screened Coulomb and exchange parameters U and J, using the relations:

$$U = F_0; \qquad J = (F_2 + F_4)/14 \quad \text{and the ratio} \;\; F_4/F_2 \sim 0.625 \tag{2.19}$$

The final ratio is obtained from numerical calculations of the Slater integrals in d-elements [9, 10].

For d electrons, the Slater integrals need only be kept through F_4, so all three needed quantities are determined once U and J are determined. These parameters can be calculated self-consistently using various constrained occupation approaches [11, 12], but are generally taken from the literature or even fit to experimental band gaps or some other observed property of the system. Without explicit calculation of U and J and an objective and self-consistent mthod of specifying the local orbitals, the LDA+U procedure cannot strictly be called a first principles approach.

Double Counting

One of the main difficulties of the LDA+U scheme is correcting for the double-counting which arises from the fact that similar interaction terms are included in the LDA.. The added orbitally-dependent potential contains interactions which are already dealt with in the mean-field correlation of the LDA. Therefore, the part of the Hubbard-like term which is sufficiently accounted for by LDA should be subtracted off. The identification of the double-counting term is difficult because standard LDA is not formulated in terms of orbitals. Presently, there are several different methods of subtracting off double-counting terms [7, 10, 13, 14]. They fall into two broad categories: double-counting for extremely localized systems where orbital occupations are approximately 1 or 0, and double-counting for systems where the spherical symmetry has been broken and orbital occupations are approximately equal. The use of the LDA+U energy functional in this research is confined to systems in which the strongly correlated orbitals are well localized, so only the first kind of double-counting will be addressed in detail here. For highly localized, correlated orbitals, the double-counting term is written:

$$E_{dc} = \frac{1}{2}Un(n-1) - \frac{1}{2}J[n_{\uparrow}(n_{\uparrow}-1) + n_{\downarrow}(n_{\downarrow}-1)] \tag{2.20}$$

where $n^{\sigma} = \mathrm{Tr}\tilde{n}^{\sigma}$ ($\tilde{n}^{\sigma}$ is the density matrix) and $n = n_{\uparrow} + n_{\downarrow}$. Combining Eq. 2.17 with Eq. 2.20, the full LDA+U energy functional, including double-counting subtractions is:

$$E^U[n] = \frac{1}{2} \sum_{\{m\},\sigma,\sigma'} n^{\sigma}_{mm'}(< m, m''|V_{ee}|m', m''' > \tag{2.21}$$

$$- < m, m''|V_{ee}|m''', m' > \delta_{\sigma,\sigma'})n^{\sigma'}_{m''m'''} \tag{2.22}$$

$$- [\frac{1}{2}Un(n-1) - \frac{1}{2}J[n_{\uparrow}(n_{\uparrow}-1) + n_{\downarrow}(n_{\downarrow}-1)] \tag{2.23}$$

The first term is the direct Coulomb interaction, the second takes into account exchange, and the final term attempts to correct for double counting of exchange and correlation in an orbitally averaged way (as in the LDA functional).

Self-consistent LDA+U

The orbitally dependent potential is derived from the LDA+U energy and double-counting terms by taking the functional derivative with respect to orbital occupation number. The full potential of the system now depends on the standard LDA potential - an $\vec{r}$-dependent functional of the density, and on the U potential which is a functional of the density matrix and is a constant shift applied to the local orbital. In each step of the self-consistency cycle, the density matrix must be calculated by projecting the desired orbitals out of the wave functions.

Using the localized double counting scheme as given in Eq. 2.20, the LDA+U functional reduces to the original LDA function when all orbitals are equally occupied, a situation which the standard LDA exchange correlation scheme is presumed to handle well.

By allowing for orbital polarization (non-uniform occupancy of orbitals), the LDA+U scheme makes investigation of systems with orbital ordering possible. The initial density matrix can be given as an input, whereby it is often possible to calculate the energy of

several different orbital occupation configurations and compare the energies associated with them. In practice, it is sometimes necessary to provide a reasonable starting density matrix. The U part of the LDA+U potential favors completely occupied or unoccupied orbitals. In partially filled shells, which orbitals are filled and which are left empty may be determined by a variety of factors, such as spin-orbit coupling or weak crystal field effects. An initial density matrix in which the wrong orbitals are substantially filled may converge to a solution in which they become completely filled while those which should be filled are moved above the Fermi energy. A comparison of the total energies of different ground state solutions should provide a mechanism by which to understand the true ground state orbital occupation.

Chapter 3

Magnetism: Localized vs. Itinerant

3.1 Itinerant Systems

The phrases delocalized, itinerant, and band-like have all come to refer to magnetic systems in which the spin-polarized density cannot be neatly assigned to a given ion or to a recognizable atomic (ionic) configuration. The extreme limit of an itinerant magnetic system would be a spin polarized uniform electron gas (with a similarly uniform positive background). The eigenstates of a non-interacting, homogeneous electron gas are plane waves and therefore maximally distributed throughout the system. If the interactions between electrons are assumed to be highly screened and treated as a perturbation, the wave functions will still be very plane wave-like and extended. In any real system, the background is not a constant positive charge density, but rather a configuration of periodic ion cores. The atomic functions which are eigenstates of isolated atoms are strongly hybridized in itinerant systems. Hybridization broadens the density of and delocalizes the electrons. The stronger the hybridization, the more the effect of the ion cores is masked and the more

band-like the magnetic picture becomes. Eventually, the plane wave picture is more accurate than the atomic picture and the magnetic moment is carried by wave functions which are spread throughout the crystal. Though exceptions exist, metallic magnets are generally of the itinerant category, while insulators are of the localized category.

An important feature of delocalized magnetic systems is the disappearance of the orbital angular momentum. The overall magnetic moment in an isolated atom is given by $\vec{M} = \mu_B(2\vec{S} + \vec{L})$, where the 2 is the spin g-factor ratio. The total angular momentum is given by $\vec{J} = \vec{L} + \vec{S}$. Hund's first, second, and third rules can be used in conjunction to determine how spin and angular momentum combine to produce the overall moment. In itinerant systems, the picture is quite different. Hund's rules which often work in extended systems, provided the orbitals are atomic-like but not necessary strictly atomic, are completely invalid when the orbitals are not well localized. The orbital angular momentum, $\vec{L}$, is no longer a good quantum number, as the electron's environment is not even approximately spherical. Electrons are not localized to any given ion core and therefore the potential they see is hugely distorted from the atomic one by the crystal electric field, caused by the static arrangement of nearest neighbor ions. This results in a cancellation of orbital angular momentums, known as "quenching". To a good degree of accuracy in many itinerant electron systems, $\vec{M} = 2\vec{S}$ and $\vec{J} = \vec{S}$ [15].

3.1.1 Treatment of Itinerant Systems

Itinerant magnetic systems are well treated by conventional first principles band theory methods. The main approximation of current DFT methods is the LDA. The LDA uses an exchange correlation potential borrowed from the homogeneous electron gas, rather

than employing the accurate (but completely unknown) non-local potential that exists in reality. The closer a real system is to the homogeneous electron gas, the less error is introduced into the calculation through use of the LDA. Delocalized electrons are generally weakly correlated with one another such that the underestimation of correlation effects inherent in the LDA does not significantly affect the accuracy of calculated properties.

Some aspects of itinerant systems can be captured by model calculations. The tight binding model can reproduce features of delocalized systems by correctly modeling the hybridization of atomic-like orbitals. However, this involves parameters which are not known beforehand (without input from a first-principles band calculation) and must be guessed or adjusted to fit experimental data. If the hybridization is due to a large number of atomic-like orbitals the fitting process can become cumbersome.

Itinerancy is not a defined property, nor can clear lines necessarily be drawn between it and localized systems. There are systems which exhibit behaviors associated with both itinerancy and localization. Certainly there is no ironclad way of identifying *a priori* whether a system is band-like enough to be modeled accurately by DFT methodology. Often, after a system is shown to be treated well by band theory, it inherits the classification of itinerant electron system.

3.2 Localized Systems

In contrast to the itinerant systems, magnetic compounds which are classified as localized have magnetic moments that are well-defined in real space. The orbitals which are spin-polarized can be localized within some radius and connected to a particular ion or ions

in the crystal. A term in the inverse susceptibility which falls off $\sim 1/\mathrm{T}$ (i.e. according to the Curie Law) can be regarded as experimental evidence of a local magnetic moment [15]. To discuss local moments in a general way, it is helpful to define two terms, with a picture of periodic ions containing atomic-like orbitals in mind. The first term is t, which describes the tendency of an electron to hop from one site to another. This tendency is governed by the overlap of orbitals located on the two sites in question. The second term is U which is the energy price (Coulomb energy) paid by two electrons which occupy orbitals on the same ion. If t is large compared to U, there is little price to be paid for double occupancy of a single site and electrons hop from site to site continuously and cannot be said to be localized. In systems where t is large, bands will disperse strongly and the density of states will be broad. In the opposite limit, U is much larger than t and the price of double occupancy is great. Electrons prefer to stay on a single ion, rather than hop to another which already contains an electron. The extent to which a system is localized can be gauged by the ratio U/t.

In a localized picture, Hund's rules apply (electrons are sharing an ion) and partially filled shells on each ion will have aligned spins. In addition, the orbital angular momentum, $\vec{L}$ is approximately a good quantum number, as the potential felt by localized electrons is approximately spherical. The total angular momentum $\vec{J}$ and the magnetic moment $\vec{M}$ will involve both the spin and angular moments. In many localized systems, particularly those involving very heavy ions, the spin-orbit interaction is extremely important and in f electron systems, it generally dominates the crystal field effect.

3.2.1 Treatment of Localized Systems

The energy U which localizes electrons is also a gauge of correlation. The exchange-correlation potential of the LDA is based on a homogeneous gas of electrons bearing little resemblance to electrons localized to specific ions. Correlation between these localized electrons will no doubt be strongly underestimated through application of the LDA. The degree to which the LDA fails in localized magnetic systems depends in large part on the extent of the localization. At a minimum, the LDA underestimates the gap in insulators, sometimes very badly. The most catastrophic failure occurs in d and f electron systems with partially filled shells. Though the d or f orbitals are often extremely localized (nearly atomic-like in some cases), the LDA ground state has each orbital equally occupied, leaving partially filled bands at the Fermi level. The LDA in this case predicts a metallic ground state for compounds which may in reality have quite a pronounced gap.

Model Hamiltonians, such as the Hubbard model, have had great success with the same systems which are badly described by the LDA. The Hubbard model is predicated on localized orbitals rather than a homogeneous gas and therefore models systems with a large U successfully. There are many models derived from or based on the Hubbard model, the vast majority of which are unsolvable except in very specific instances. Nonetheless, some of these specific instances are very important and the Hubbard model and its derivatives are an invaluable tool for insight into localized magnetism.

Chapter 4

Three Magnetic Systems

The three systems described in this chapter exhibit different degrees of localization, beginning with rather delocalized-localized and moving to extremely localized. In each case, model systems appropriate to the kind of magnetism being studied and to the specific compound are applied. A description of each compound and the motivations for its study are given here, along with a brief discussion of the appropriateness of the LDA in each case.

4.1 $MgCNi_3$

$MgCNi_3$ is a metal which becomes a superconductor at around 8 K and is not magnetic. Several features of the material suggest nearness to ferromagnetism and it is this possibility which is investigated. The study of nearby magnetic phases is partially motivated by the presence of a surprisingly substantial amount of Ni (one of the few elemental magnets) for a superconducting compound. If a magnetic phase can be shown to be near the superconducting ground state, the intriguing possibility of a transition to this state

while still within the superconducting phase arises. The coexistence of superconductivity and magnetism is a phenomenon which has recently been experimentally verified [16, 17] and has spurred an enormous amount of research into the details of how two such normally antagonistic phases could occur simultaneously.

The Ni-d electrons in this compounds are strongly hybridized with C-p orbitals and to some extent with one another. Any magnetic phase of this compound would fall under the category of band ferromagnetism. The magnetic moment of a band ferromagnet arises due to the spin alignment of delocalized conduction electrons. This type of magnetism is generally well-treated by the LDA, and DFT methods have in the past accurately predicted the onset of band ferromagnetism as well as the correct ground state moment. Inaccuracies in the exchange-correlation potential are unlikely to cause calculated ground state properties to differ substantially from experimental results.

4.2 $CaCu_3Ti_4O_{12}$

$CaCu_3Ti_4O_{12}$ (CCTO) is an insulating compound with an unusually high dielectric constant. In addition, the high value is nearly temperature independent from T= 298 K to T= 572 K, making it very attractive for device purposes. Though the dielectric properties of CCTO stimulated the initial research into the compound, its magnetic ordering mechanism is the motivation for the study here. At T = 25 K, a simple Néel antiferromagnetic order emerges. The magnetic moment is due to an unpaired spin localized to the Cu site, and the magnetic orbitals are largely d-like in character, though much hybridization with other orbitals is present. The magnetic interactions in CCTO are complicated by its structure

which dictates that nearest and next-nearest neighbor orbitals are orthogonal. Thus, the simple nearest (magnetic) neighbor superexchange picture cannot account for the anti-alignment of nearest neighbor spins.

The magnetic d bands of transition metals present a rather difficult computational problem because they exhibit both localized and delocalized-localized properties, both of which are essential to the physical behaviors associated with them. The LAPW basis set is, to date, the most accurate method of treating transition metal bands because it is flexible enough to represent the fluctuating charge density inside the spheres as well as the more slowly varying density in the interstitial. The insulating gap of CCTO is not at all well reproduced by the LDA calculation, but the failure is not extreme enough to produce a metallic ground state. The correlated d-bands could possibly be better treated using LDA+U, but the effect would likely be to rigidly shift the occupied magnetic bands downward and the unoccupied upward. Since the magnetic properties of interest will depend only on the shape of the bands and not their exact position in the energy spectrum, the standard LDA approach has been used.

4.3 EuN

EuN is a very simple compound; it has two atoms per unit cell and takes the rocksalt configuration. Very little is known experimentally about the compound and the main interest in studying it is derived from the configuration of its partially filled f-shell. The formal valency of this compound is Eu^{3+} N^{3-}, which leaves the Eu ion in a f^6 configuration. The f orbitals are very localized such that a spherical potential approximation is good. In

this situation, Hund's rules apply and dictate that all six spins should align ($|S_{ztot}| = 3$), the l_z levels -3 through 2 should be filled ($|L_{ztot}| = 3$) , and that the total angular momentum should be $\vec{J} = |\vec{L} - \vec{S}| = 0$. With an overall $\vec{J} = 0$, the compound is non-magnetic. However, at each site, there is a very large spin moment. Exchange interactions which proceed via spin-spin ($\vec{S}_i \cdot \vec{S}_j$; i, j label sites) mechanisms, in contrast to $\vec{J}_i \cdot \vec{J}_j$ mechanisms, should be present and could cause a sort of invisible ordering (this is described more fully later) in which the z-components of all spins are aligned (or anti-aligned) and likewise the z-components of all orbital angular momentum vectors ordered, with spin and orbital angular momenta canceling one another at each site.

In order to investigate magnetic interactions and possible magnetic interactions in this ostensibly non-magnetic compound, the LDA+U procedure must be used. A straightforward LDA calculation yields an incorrect metallic solution with the partially filled Eu-f bands at the Fermi energy (a very well known problem with LDA). With the LDA+U implementation, several different solutions are stable, depending on the initial density matrix (assumed ionic configuration). Distinguishing between these configurations necessitates the use of spin-orbit coupling, the effects of which are very important to the orbital polarization.

Chapter 5

$MgCNi_3$

5.1 Introduction

The simple compound $MgCNi_3$ was first found to superconduct at ~ 8 K by He *et al* [18]. The compound is Ni based and can be thought of as fcc Ni with one out of every four Ni atoms replaced with Mg and a C atom added in the empty center site. Since fcc Ni is a strongly magnetic compound, the absence of magnetism and the presence of superconductivity in the very similar structure of $MgCNi_3$ were highly surprising. Since the lattice constant of fcc Ni is smaller than that of $MgCNi_3$ and hence the Ni-Ni distance is smaller, there is reason to think that manipulation by pressure or by some other means might drive this compound to a ferromagnetic state. Additionally, electronic structure calculations show a sharp peak in the density of states very near the Fermi energy, providing another reason to investigate the possible proximity of magnetism. Because of the close structural similarity, methods which correctly predict and interpret the magnetic behavior of Ni are expected to work well also for $MgCNi_3$. The (proposed) magnetic moment would

be delocalized and band-like - an ideal system for investigation with density functional methods. The correlation effects modeled by the LDA should be sufficient to capture the relevant physics, though non-local exchange-correlation effects should always be kept in mind. To supplement the first-principles calculation, the Stoner model of magnetism will be applied. This model is also well-suited to band ferromagnetism and often accurately predicts not only the onset of magnetic behavior but also the correct moment in comparable compounds.

5.2 Structure

$MgCNi_3$ has an anti-perovskite structure. In a typical perovskite, ABO_3, a transition metal with d states sits at the center (B) site, and oxygen atoms with s and p states occupy the faces. The A site is generally a metal cation of non-transition metal type. In an anti-perovskite, the central and face positions are reversed. The B site is occupied by an atom with s and p valence states, while the faces contain transition metal ions with d states.

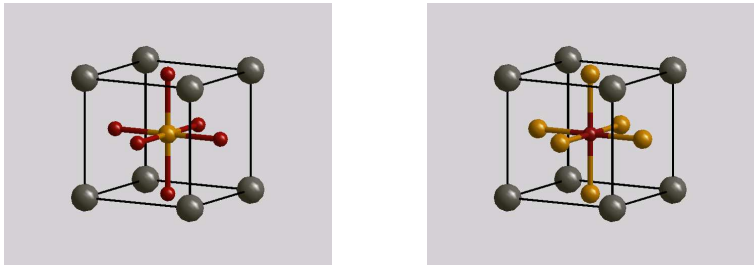

Figure 5.1: *left side* Typical perovskite structure: the gold sphere at the center represents a transition metal ion and the red spheres on the faces represent an ion with s and p states, usually oxygen.*right side* Anti-perovskite structure: the gold spheres (still representing transition metal ions) have moved to the faces while the red sphere (now less commonly oxygen, but still an ion with primarily s and p orbitals) occupies the center position.

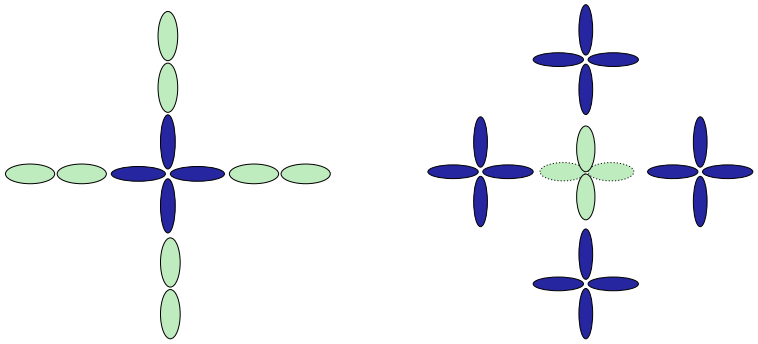

Figure 5.2: View of the (100) plane in a typical perovskite *left* and in the anti-perovskite *right*. In the anti-perovskite the $dp\sigma$ bonding is still present, but an additional $dd\pi$ bonding is also possible due to the proximity of the Ni ions to one another.

The $dp\sigma$ and $dp\pi$ bonding which characterizes the band structure of a conventional perovskite remains very important in the anti-perovskite structures. Significant differences between the two types emerge in the hopping between transition metal orbitals. Bonding between d orbitals is practically non-existent in the standard perovskites since the transition metal ions are separated by a full lattice constant. However, in the antiperovskite, the d-band ions are on the faces, separated by a distance of only $\frac{a}{\sqrt{2}}$ (where a is the lattice constant), giving rise to some dispersion due to non-zero d-d hopping integrals.

5.3 Electronic Structure

Calculations on this compound were carried out using a density functional theory code in the LAPW implementation [19] (Wien97.8). The RKmax which controls the cutoff for the planewave expansion was set to 8.00, resulting in a basis set of nearly 600 LAPW's, a rather large number for a unit cell of this size. Local orbitals were included to deal with the semi-core states of both Mg and Ni. The generalized gradient approximation [20] was used

for the exchange-correlation potential and over 800 points from the irreducible Brillouin zone were calculated. The muffin tin radius for each ion was 1.8 a.u. The structure was relaxed to determine the equilibrium lattice constant and to compare with the experimental value (see Bulk Modulus section), but throughout these calculations the experimentally determined value, a = 7.204 a.u., was used.

The electronic structure of $MgCNi_3$ has one very striking feature: a sharp peak in the density of states, located only 45 meV below the Fermi energy. This van Hove singularity has its origin in a flat band in the band structure, located around the M point of the Brillouin zone. The bands here and elsewhere near the Fermi energy are primarily Ni-d bands. An orbitally projected DOS plot reveals that $\approx$ 80 % of the weight in the peak has Ni-d character. The inset of Fig. 5.5 highlights the preponderance of Ni states in the peak.

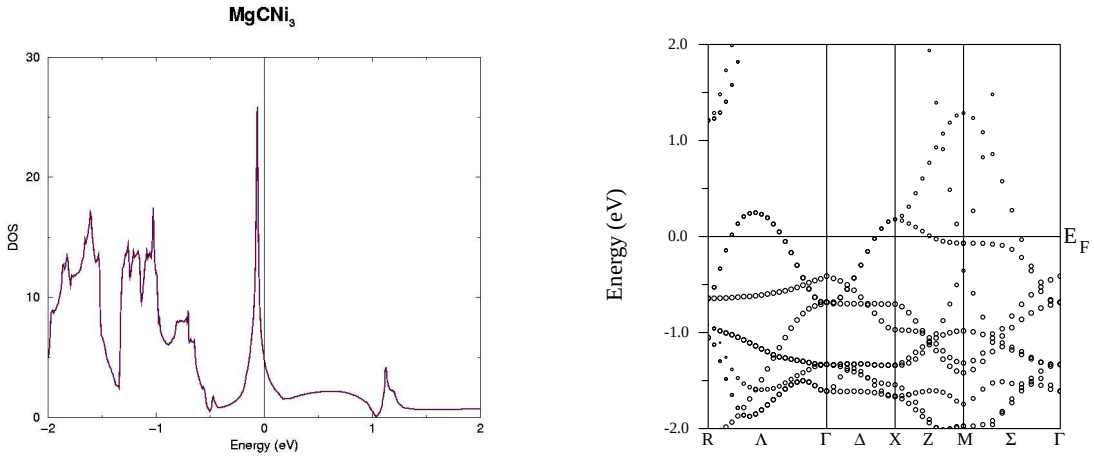

Figure 5.3: *left panel* The DOS of $MgCNi_3$. The prominent peak just below the Fermi energy is due to a van Hove singularity. *right panel* The flat band centered on the M point is responsible for the peak.

The effective masses at the van Hove singularity are remarkably large: $m^* \approx 15$

from M - X, $m^* \approx$ -15 from M - R, and m^* is effectively infinite along M - Γ: the band is *constant* to within 0.2 meV for a distance of almost $\frac{1}{3}\frac{\pi}{a}$. Away from the M point van Hove singularity, the bands are much more highly dispersive. A surface plot of the van Hove singularity is given in Fig. 5.4. The negative effective mass sheet is in a direction perpendicular to the chosen plane of the Brillouin zone and cannot be seen.

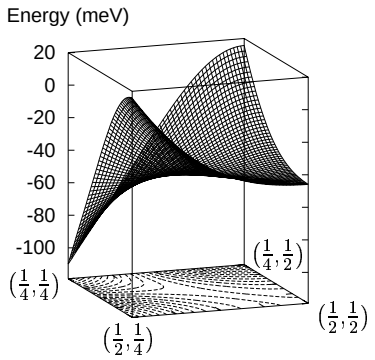

Figure 5.4: The Γ - X - M plane of the Brillouin zone. The M point is located at the right corner, labeled $(\frac{1}{2},\frac{1}{2})$. Note the extremely flat region along the diagonal.

In order to gain insight into the role of the Mg atom, the electronic structure of the fictitious compound $\square^{+2}$CNi3 was studied. This compound has no actual ion at the (0,0,0) position, but nonetheless retains the same number of valence electrons as $MgCNi_3$. The band structures of the original and fictitious compounds are nearly identical as can be seen in Fig. 5.5.

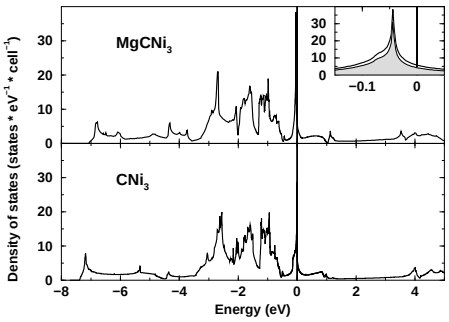

Figure 5.5: A comparison of the DOS of $MgCNi_3$ and $\square^{+2}CNi_3$. The inset is a blowup of the peak for $MgCNi_3$ with the contribution from Ni-d states shaded to show the dominance of Ni character at the van Hove singularity.

The particular shape of the Mg orbitals obviously has no bearing on the electronic structure, as they are ultimately empty and located significantly above the bands of interest. The Mg ion simply acts as a donor, giving up its electrons to the Ni-d states. A similar calculation replacing the C atom by only its valence electrons reveals that the specific structure of the carbon p-states is vital to the band structure of $MgCNi_3$. This result suggests that doping at the Mg site will induce a rigid-band shift of the electronic structure while doping at the C site will fundamentally affect the shape of the DOS. This important information will be used in conjunction with the Stoner model to investigate the possible proximity of ferromagnetism.

5.4 The Stoner Model

In the single-particle picture, magnetic transitions can be understood as the competition between the exchange energy, which favors unbalanced spin occupations, and the energy price paid by aligned electrons which must occupy higher single particle eigenstates

due to the Pauli exclusion principle. The Stoner model [21, 22] formulates the energy of magnetic systems based on this competition, subsuming detailed information about the exchange interaction into a single parameter, the Stoner I. The Stoner model works well for the zero temperature magnetic moment of delocalized-localized or band ferromagnetism where the single particle picture also works well, i.e. in weakly correlated systems. The model requires the input of an accurate band structure calculation to supply information about the distribution of energy states. To investigate the possible onset of ferromagnetism in $MgCNi_3$, we will use the band structure obtained from LAPW calculations.

The LAPW band structure provides an accurate paramagnetic density of states, $N(\epsilon)$, which is the starting point for determining the energy associated with a magnetic transition. In the paramagnetic case, the up and down densities of states are equal. To move from a non-magnetic state to a magnetic one, the occupation of the up spin states must differ from that of the down spin states, i.e. the DOS of the two spins must be shifted with respect to one another and the Fermi energy. For one spin, electron states previously below the Fermi energy will become unoccupied and for the other spin, states that were unoccupied above the Fermi level will be filled.

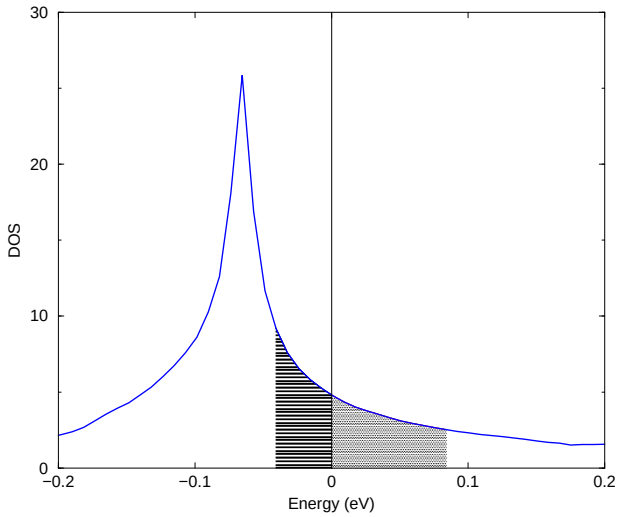

Figure 5.6: Blowup of the paramagnetic DOS of $MgCNi_3$ near the Fermi energy. Removing electrons from below the paramagnetic ϵ_F in the down DOS (darkly shaded region) and filling states above the paramagnetic ϵ_F (lightly shaded region) results in an overall non-zero magnetic moment. Shaded regions have the same area above and below the Fermi energy to conserve electron number. States which become empty are of minority spin type, while states that are filled are of the majority spin type

The removal of electrons from low energy states and their replacement in higher energy states causes an overall increase in kinetic energy which depends on the number of electrons which are moved and the shape of the DOS. Because the magnetization, M, is given by the difference between the number of up and down electrons in the system, the energy of transferring electrons, E_t, can be formulated in terms of M.

$$E_t(M) = \underbrace{\int_{\epsilon_F}^{\epsilon(M)} \epsilon' N(\epsilon) d\epsilon}_{\text{filled states}} - \underbrace{\int_{\epsilon(-M)}^{\epsilon_F} \epsilon' N(\epsilon') d\epsilon}_{\text{emptied states}} \tag{5.1}$$

$$\text{where } \epsilon(M) \text{ is defined by} \quad \int_{\epsilon_F}^{\epsilon(M)} N(\epsilon) d\epsilon = M/2$$

The $\epsilon_F \equiv \epsilon(\text{M=0})$ in the limits of the integration refers to the Fermi energy of

the paramagnetic system; $\epsilon(M)$ is the energy of the highest filled majority spin state, and $\epsilon(-M)$ is the energy of the lowest unfilled minority spin state. The energy, E_t, does not take into account any change in the DOS that might be caused by the magnetization and hence the exchange potential, being associated primarily with the Ni atom. This energy, along with the compensating exchange energy are given by $E_I = -\frac{1}{4} I M^2$. The details of the band structure change and the specific electron-electron exchanges are contained in the Stoner parameter, I, which in general will depend on the magnetization. The energy E_I is even because, in the absence of an external magnetic field, the overall energy of the system cannot depend on whether it is spin up or spin down electrons which are shifted into higher energy states. This model does not deal with any higher order even terms, though they may exist. The total energy, E_{mag}, associated with the magnetization of the system is the sum of E_t and E_I. If, for some M, the E_I term dominates the E_t term, the ground state will be magnetic.

The second line of Eq. 5.1 can be rearranged in differential form as $\frac{dM}{d\epsilon} = 2N(\epsilon)$. This expression can be inserted into the first line to yield:

$$\begin{aligned} E_t(M) &= \frac{1}{2}\int_0^M \epsilon(M')dM' - \frac{1}{2}\int_{-M}^0 \epsilon(M')dM' \\ &= \frac{1}{2}\int_0^M \frac{M'dM'}{\overline{N}(M')} \\ \overline{N}(M) &\equiv \frac{M}{\epsilon(M) - \epsilon(-M)} \end{aligned} \tag{5.2}$$

$\overline{N}(M)$ can be thought of as an averaged density of states, corresponding to moment M. M/2 is the number of electrons that are moved and the $\epsilon(M') - \epsilon(-M')$ is the energy interval over which they are moved. At M=0, $\overline{N}(M=0) \longrightarrow N(\epsilon_F)$. Now E_{mag} can be

put in its final form, often called the extended Stoner model:

$$E_{mag} = \frac{1}{2}\int_0^M \frac{M'dM'}{\overline{N}(M')} - \frac{1}{4}I(M)M^2 \tag{5.3}$$

The second derivative of E_{mag} yields the inverse susceptibility, $\chi^{-1}(M) = \frac{d^2E_{mag}}{dM^2}$. Assuming that $\frac{dI}{dM} = 0$, and evaluating at M = 0

$$\chi(0) = \frac{2\mu_B N(\epsilon_F)}{1 - N(\epsilon_F)I} \tag{5.4}$$

The factor 1/(1 - N(ϵ_F)I) multiplies the bare (Pauli) susceptibility $\chi_0 = 2\mu_B N(\epsilon_F)$ and is known as the Stoner enhancement. When its value becomes infinite, the Stoner criterion IN(ϵ_F) = 1, is fulfilled, and the M=0 state is unstable to ferromagnetism. Information about the moment of the resulting magnetic ground state can also be obtained from the Stoner formulation by minimizing E_{mag} with respect M (again assuming that I is independent of M)

$$\frac{dE_{mag}}{dM} = \frac{1}{2}\left(\frac{M}{\overline{N}(M)} - IM\right) \tag{5.5}$$

Upon setting this derivative equal to zero, the condition for a magnetic state emerges (the second derivative must be positive to ensure stability):

$$\overline{N}(M_C)I = 1 \qquad M_C = \text{critical magnetization} \tag{5.6}$$

If the DOS is nearly constant around the Fermi energy, then the approximation $\overline{N}(M) \approx N(\epsilon_F)$ is valid and the equation reduces to the Stoner criterion. If Eq. 5.6 cannot be satisfied for *any* value of M, then the energy gain due to shifting the up and down

densities of states cannot be compensated for by the exchange energy and the system will be paramagnetic.

5.5 Application of Stoner Model to $MgCNi_3$

The Stoner criterion requires two inputs which can be obtained from band structure calculations. The first is the DOS and the second is the parameter I. With these two quantities, a determination of whether the system has a magnetic ground state or not can be made. In the case of $MgCNi_3$, the ground state has already been determined both experimentally and theoretically to be paramagnetic. The DOS of $MgCNi_3$ is not particularly high at the Fermi energy and the Stoner criterion is evidently not fulfilled. However, the sharply rising DOS hints that the system may be very near to ferromagnetism and that manipulating the Fermi level through hole-doping or pressure could drive the system to a ferromagnetic state. This possible nearness to ferromagnetism can be explored using the calculated paramagnetic DOS and the Stoner model.

5.5.1 Calculating the Stoner Parameter

There are two ways to calculate the parameter I, using first-principles band theory calculations. The first is to use the calculation of a second material, $Mg_{0.5}Li_{0.5}CNi_3$, which has a magnetic ground state, to determine exchange splitting between majority and minority spin bands and calculate the Stoner parameter with the relation $E_{ex} = IM$. As we have shown, the Mg ion is simply an electron donor and its particular chemical character has no real effect on the band structure. The I from $Mg_{0.5}Li_{0.5}CNi_3$ should carry over well into

other $X\mathrm{CNi_3}$ calculations, provided I is, as assumed, independent of the magnetic moment (any dependence on M will be second order so the assumption is generally very good). The exchange splitting in $\mathrm{Mg_{0.5}Li_{0.5}CNi_3}$ is 0.25 eV, as can be seen by looking at the distance between up and down peaks in Fig. 5.7. The calculated magnetic moment of this compound is 0.85 eV, giving a Stoner parameter of 0.29 eV.

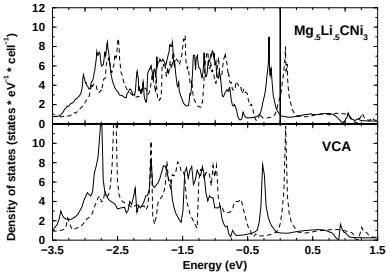

Figure 5.7: *top panel* The DOS of $\mathrm{Mg_{0.5}Li_{0.5}CNi_3}$ obtained through a super-cell calculation with alternating Mg and Li layers. *bottom panel* A virtual crystal calculation of the DOS for $\mathrm{Mg_{0.5}Na_{0.5}CNi_3}$, where each site is occupied by a fictitious atom of atomic number 11.5.

The second method of determining the Stoner parameter comes from using the definition of inverse susceptibility to write

$$E_{mag} = \frac{1}{2}\chi^{-1}M^2 \tag{5.7}$$

which should hold for small M. The E_{mag} vs. M curve can be generated using the fixed-spin moment procedure and the quadratic coefficient determined by a fit to this curve. At small M, the curve is nearly perfectly quadratic with a coefficient of 0.28 eV/μ_B, which agrees extremely well with the value calculated from the exchange splitting of $\mathrm{Mg_{0.5}Li_{0.5}CNi_3}$. For further use in Stoner model calculations, the parameter I is taken to be 0.29 $\frac{eV}{\mu_B}$, an average of the results from the two methods.

Though it doesn't yield any information about the value of the magnetic moment expected in the ground state, applying the Stoner criterion reveals that an $N(\epsilon_F) = 3.45$ $\frac{states}{eV\,spin}$ is needed to make the ground state unstable toward ferromagnetism. Due to the rapidly rising DOS, this could be achieved if the Fermi energy were shifted downward by 26 meV.

5.5.2 Manipulating the Fermi Energy

Pressure

Studying the pressure dependencies of $MgCNi_3$ show that it is remarkably insensitive to compression or expansion. The effect of compression is very small and results in a rigid downward shift of the DOS at the rate of 0.31 $\frac{meV^{-1}}{a.u.^3}$. In Fig. 5.8, a compression of 5 % by lattice parameter (quite large by experimental standards) causes a nearly imperceptible shift in the density of states, particularly near the Fermi energy. The amount of pressure represented by this scale of compression requires knowledge of the bulk modulus. This can be calculated from $B = V\frac{\partial^2 E(V)}{\partial V^2}$ (where E(V) is the total energy at a given density) and an energy vs. volume curve. The calculated data points for different volumes and the fit to the curve [23] which gives B = 214 GPa are shown in Fig. 5.8.

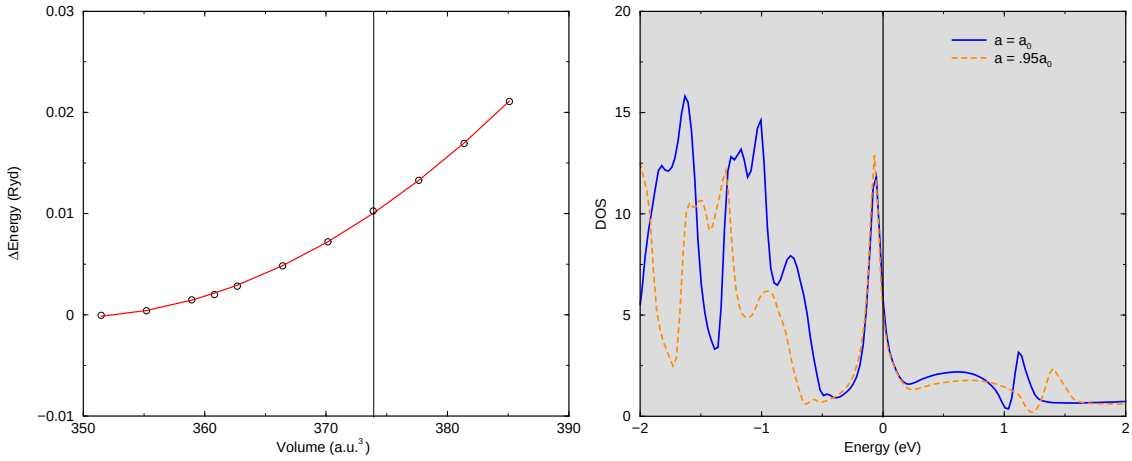

Figure 5.8: *left panel* Energy vs. Volume curve for $MgCNi_3$. The vertical line represents the equilibrium volume. The curvature gives the bulk modulus. *right panel* The effect of pressure on the band structure of $MgCNi_3$. When the volume is compressed by 14%, the peak remains almost unchanged in height and in position relative to ϵ_F

Using this bulk modulus and assuming the rate at which applied pressure shifts the spectrum remains constant (i.e. even large pressures do not fundamentally change the shape of the band structure), we find that a 'negative pressure' of 48 GPa would be needed to move the DOS at ϵ_F high enough to satisfy the Stoner criterion. While this type of pressure is not unreasonable experimentally in terms of compression, negative pressure can only be applied by employing so-called chemical pressure. Chemical pressure is achieved by replacing one atom by an isovalent but larger one. $MgCNi_3$ would be an ideal system for this type of pressure at the A-site, but the extent to which the compound must be expanded is far beyond what could be hoped for with this method. Pressure is simply not a useful tool for inducing a magnetic transition in $MgCNi_3$.

Hole-doping

A second method for moving the Fermi energy down is hole-doping. Two theoretical methods are used to investigate the effects of doping on the band structure and its consequences for the possible magnetism of the compound 1) A Stoner analysis using the paramagnetic band structure 2)A series of virtual crystal calculations. Both methods are justified by the rigid-band behavior of $MgCNi_3$ with respect to changes in the chemical composition of the A-site (see Figs. 5.5 and 5.7).

Stoner analysis

Assuming that the removal of electrons through doping causes a rigid upward shift of the band structure relative to the Fermi energy, a Stoner analysis for various dopings was performed. Using DOS information from the paramagnetic calculation on a very fine energy mesh, the averaged density of states, $\overline{N}(\mathrm{M})$, and E_{mag} (Eq. 5.7) are calculated for various dopings of $MgCNi_3$. The doping is simulated by rigidly shifting the spectral density by an amount which represents the number of electrons to be removed from the system through Li or Na substitution. The results of the calculations can be analyzed in two ways. The first is to simply track the energy vs. magnetic moment to find the minimum for each doping. For small dopings, the energy increases monotonically away from the $\mathrm{M} = 0$ state, but for dopings beyond the critical doping, the energy dips below zero and hits a minimum before returning again to positive values. Graphing various doping levels vs. magnetic moment shows that the curve first begins to dip below zero around $\delta = 0.12$.

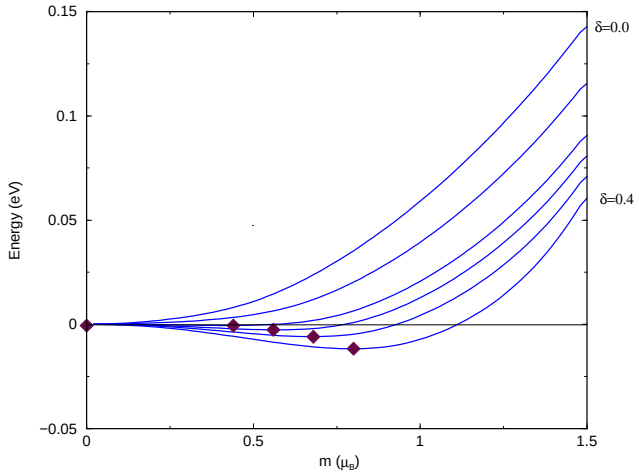

Figure 5.9: Energy vs. M curves for various dopings. The black diamonds mark the minimum of the curve, signifying the moment of the magnetic ground state. For small dopings, the minimum is at zero (no moment), but around $\delta = 0.12$, a non-zero magnetic moment becomes energetically favorable.

The second method of analysis makes explicit use of the Stoner criterion by comparing the averaged density of states to the quantity 1/I for increasing magnetic moment at each doping. When the hole-doping is sufficient to produce a magnetic ground state, $\overline{N}$(M) will be equal to 1/I for some M, fulfilling the condition for ferromagnetism.

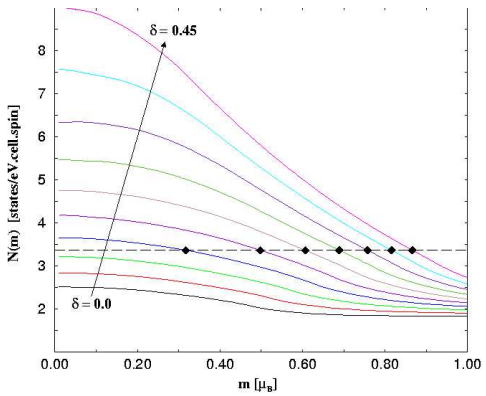

Figure 5.10: $\overline{N}$(M) vs M, the intersection of this curve with the line 1/I indicates the predicted magnetic moment of the ground state

An expression for the dependence of M_C (the magnetic moment of the ground state) on the doping parameter can be derived analytically by Taylor expanding the averaged density of states with respect to δ and M and setting the result equal to 1/I.

$$\overline{N}(M, \delta_{cr}) \approx \overline{N}(0, \delta_{cr}) + \frac{d\overline{N}(0, \delta_{cr})}{d\delta}(\delta - \delta_{cr}) + \frac{1}{2}\frac{d^2\overline{N}(0, \delta_{cr})}{d^2 M}M^2 = I^{-1} \tag{5.8}$$

and noting that $\overline{N}(0, \delta_{cr}) = 1/\mathrm{I}$. The result is a magnetic moment which grows as $\mathrm{M}(\delta) = \mathcal{G}(\delta - \delta_{cr})^{\frac{1}{2}}$ with

$$\mathcal{G} = \left| \frac{d\overline{N}(0, \delta_{cr})}{d\delta} \Big/ \frac{d^2\overline{N}(0, \delta_{cr})}{d^2 M} \right|^{\frac{1}{2}} \tag{5.9}$$

The resulting curve is plotted along with the virtual crystal calculations for comparison in the next section. The intersection of the curve with the M=0 axis gives the critical doping, δ_{cr} (See Fig. 5.11).

Virtual Crystal Calculations

Spin-polarized calculations were performed for a range of dopings at the Mg-site, using the virtual crystal approximation (VCA) for $Mg_{1-\delta}Na_{\delta}CNi_3$. The VCA approximates $Mg_{1-\delta}Na_{\delta}$ by a fictitious element with atomic number Z= Z_{Mg}(1-δ) + $Z_{Na}\delta$. In the case of doped $MgCNi_3$ compounds, this approximation is justified by the rigidity of the bands with respect to changes at the Mg site. Once self-consistency was reached in each doping case, the magnetic moment was calculated. A graph of this moment vs. doping parameter, δ, is given in Fig. 5.11 , along with the single supercell calculation data point $Mg_{0.5}Li_{0.5}CNi_3$, and the derived quadratic curve, Eq. 5.9.

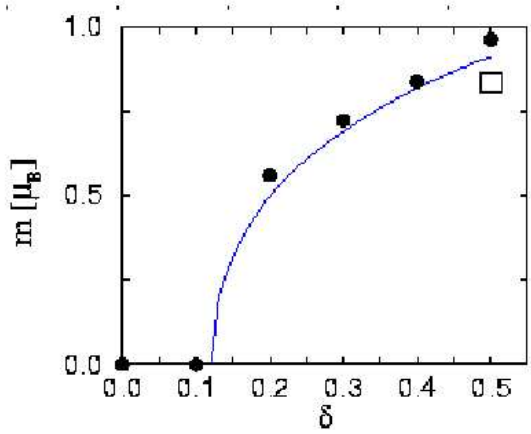

Figure 5.11: Virtual crystal calculations for $MgCNi_3$. The data point for the supercell calculation of $Mg_{0.5}Li_{0.5}CNi_3$ is included, showing that VCA and super-cell calculations are very similar.

The graph shows that both virtual crystal calculations and the Stoner analysis give results that are consistent in predicting the onset of ferromagnetism at a critical doping of $\delta_{cr} = 0.12$. The more accurate super-cell calculation also falls very near the curve, further confirming the results. Unfortunately, such doping has so far resisted experimental attempts to incorporate Na into $MgCNi_3$.

Chapter 6

$CaCu_3Ti_4O_{12}$

6.1 Introduction

$CaCu_3Ti_4O_{12}$ (CCTO) is an anti-ferromagnetic insulator which has an extremely high, nearly temperature independent (for a wide range of temperatures) dielectric constant [24]. This property, which is potentially useful technologically, is now thought to be an extrinsic effect [25] but has nonetheless generated much interest in CCTO as well as in compounds which share its structure class, the "quadruple perovskite". The quadruple perovskite structure also has important ramifications for the magnetic ordering of CCTO. The compound orders at a temperature of $\sim$ 25 K [24, 26] into a very simple Néel configuration - each spin is anti-aligned with all of its nearest neighbor spins. The exact origin of this AFM order is unclear since the Cu-O-Ti-O-Cu path that leads from one Cu site to the next has exactly the same length regardless of whether it connects 1^{st}, 2^{nd}, or 3^{rd} neighbors, though absolute distance between the neighbors differs substantially. Estimates as to the relative magnitudes and even the signs of the exchange constants J_1, J_2, J_3, which determine

the energy associated with spin alignment, vary widely. Lacroix [27] calculates the three J's (using formulas based on transfer integrals and several Coulomb parameters), assuming that only the Cu-Ti-Cu superexchange process is important. Using the non-collinear spin arrangement of Collomb *et al* [28] and including spin-orbit effects, the relative magnitude of J_3 emerges as the largest, with all three parameters positive. If the spins are allowed to be perfectly collinear, the same calculations produce J_3 ¿ J_1, J_2 , but with J_2 negative and significantly smaller than the other two. Using three magnon peaks from their Raman spectroscopy measurements and a Heisenberg Hamiltonian, Koitzsch *et al* [29] find oppositely that $|J_1| > |J_2|, |J_3|$ and that all interactions are anti-ferromagnetic. Kim *et al* [30] consider both scenarios and are unable to distinguish between them by fitting to neutron scattering measurements of the optical Gamma point magnon. The situation is made more interesting with the realization that 1^{st} and 2^{nd} neighbor superexchange coupling constants are zero by symmetry. To investigate the magnitudes of various magnetic interactions in this compound, we will combine our accurate LAPW results with several model calculations.

6.1.1 Structure

The structure of CCTO has been determined by both accurate neutron powder and x-ray diffraction experiments [31, 24, 26]. It can be understood as a derivative of the simple perovskite, $CaTiO_3$.

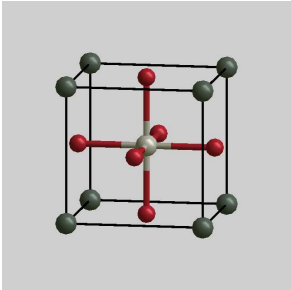

Figure 6.1: Perovskite $CaTiO_3$: The corner ions are Ca, the center is Ti, and those on the face are O.

When the formula unit is quadrupled and three out of every four Ca atoms is replaced by a Cu atom, resulting in a bcc super-cell, the compound achieves the stoichiometry of CCTO. The final step is a rotation of each of the four resulting TiO_6 octahedra around a ¡111¿ direction such that each Cu ion is four-fold coordinated with O ions in a planar CuO_4 plaquette and each octahedra remains with one triangular face perpendicular to a (111) axis. The plaquettes are very nearly, but not exactly, square - each Cu-O distance is equal, but the O-Cu-O angles differ from 90 degrees slightly. There are three different orientations of the CuO_4 plaquettes: xy, xz, and yz. The entire lattice is bcc and belongs to spacegroup Im3. The set of plaquettes with a single orientation comprises a sublattice which is also bcc, such that the CCTO structure can be thought of as the inter-penetration of three bcc sublattices, each containing only a single orientation of CuO_4 plaquettes.

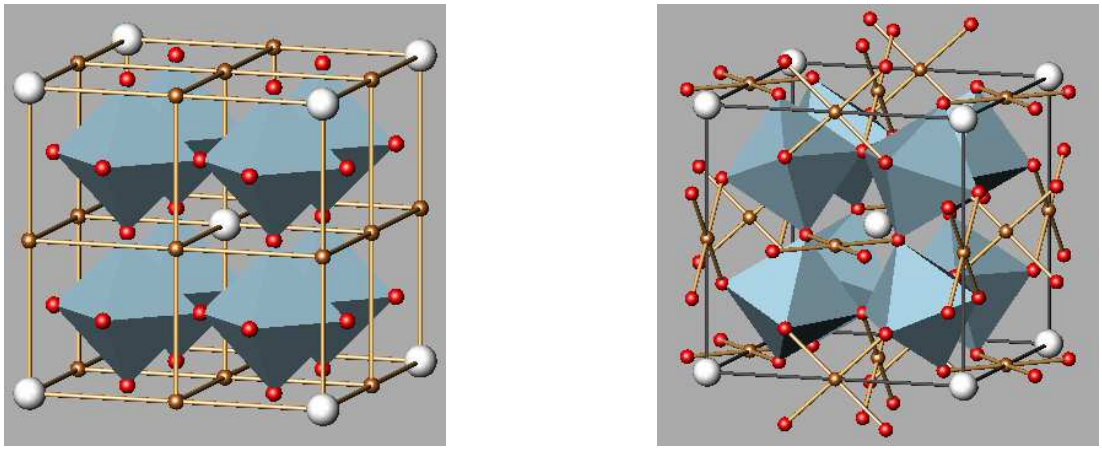

Figure 6.2: The quadruple perovskite has 20 atoms per unit cell $(ABO_3)^4$ *left side*: Quadruple perovskite with Cu ions replacing three out of four Ca. *right side*: Octahedra are tilted such that nearly square CuO_4 plaquettes with planar orientations are formed

The formal valency of CCTO is: Ca^{2+}, Cu^{2+}, Ti^{4+}, O^{2-}. This leaves each Ti ion in a d^0 configuration and as such, it would not participate in the magnetism of the compound. Each Cu^{2+} ion is in a d^9 configuration with one unpaired electron. The magnetic order stems from the anti-alignment of the single ($S = \frac{1}{2}$) spin on each Cu site with all of its nearest Cu neighbors.

6.2 First-Principles Calculation

6.2.1 Calculational Methods

Calculations were carried out using the (LAPW) method of WIEN97.8 [19]. The exchange-correlation potential of Perdew and Wang (92) [32] was used and over 3800 LAPW's were employed in the basis set. The muffin tin radii (in Bohr) were selected to be: 2.0 for Ca, Cu and Ti, 1.6 for O; the RKmax was set to 7.0. In transition metal

oxides, there is often the question of whether corrections to the local density approximation are necessary to obtain a reasonable description, with the answer being guided by experimental data. While some corrections may be necessary for this compound, the results we have obtained have the right magnetic character and are insulating, hence we expect they are useful in beginning the interpretation of their observed behavior.

Experimental data [26] for the lattice parameter and ionic positions were used: a= 7.3843Å, $(y = 0.3033, z = 0.1790)$ for the O position. To reproduce the experimentally observed AFM order for CCTO, the unit cell was doubled to allow a different magnetic state on Cu ions that would otherwise be identical. This doubling resulted in a simple cubic cell of 40 atoms; space group $Pm\overline{3}$. The calculation was performed first using the fixed-spin moment procedure, with the moment held to zero, which tends to enforce antiferromagnetic ordering. Once a reasonable charge density was reached, the calculation was allowed to proceed to self-consistency with no restriction on overall moment. The final total moment indeed converged to zero and an antiferromagnetic ground state resulted.

6.2.2 Electronic Structure

Our calculation correctly reproduces the observed AFM insulating character of CCTO. The gap in the band structure is only 0.2 eV, considerably smaller than the experimental value [33] which has a lower limit of 1.5 eV, but such underestimation of the gap is common in LDA calculations and arises from underestimation of correlation effects. Typically, the band character and shape on either side of the gap are nonetheless given reasonably. The band structure reflects the six bands, associated with six Cu ions, that are responsible for the magnetism of the compound.

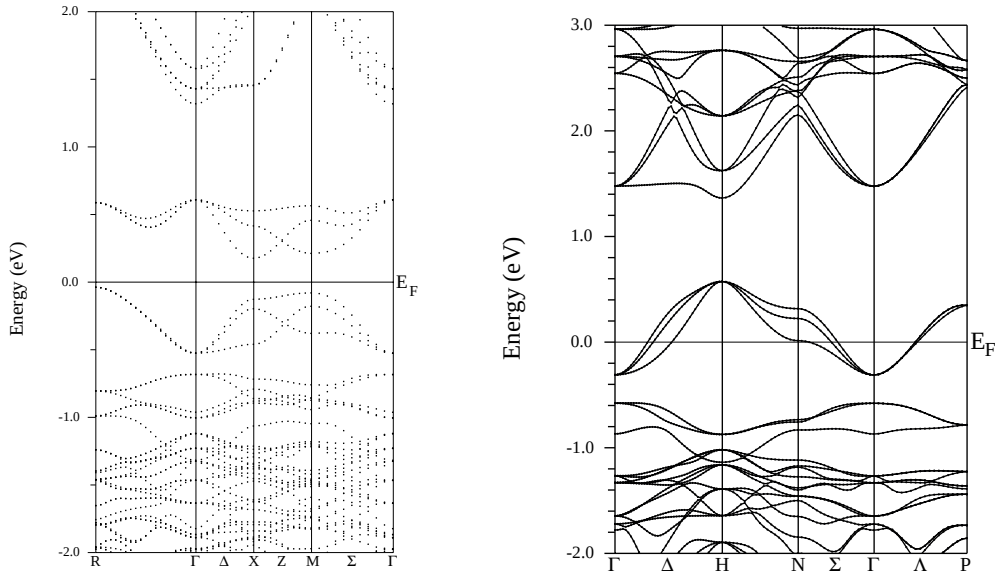

Figure 6.3: Band structure of CCTO. *left side* AFM (doubled cell) band structure; the spin-up and spin-dn band structures are identical, though filled states of spin-up bands will be mainly due to one Cu ion and filled states of spin-down bands mainly due to the other Cu ion. *right side* Paramagnetic band structure of bcc structure, the corresponding Brillouin zone is fcc. Since the magnetic orbital of each Cu site is half-filled, the ground state is erroneously metallic.

The magnetic bands are separated in energy from other bands which makes them good candidates for representation through the tight-binding model (see Tight-Binding section). The magnetic moment is mainly located on the Cu site, though the O ions in each CuO_4 plaquette have a small spin polarization in the same direction as the Cu ion to which they are attached. As in many cuprates, the hole in the Cu $3d$ shell (the magnetic orbital) involves the $dp\sigma$ anti-bonding combination of the Cu d_{xy} and the four neighboring O $p\sigma$ orbitals.

A projected density of states plot (Fig. 6.4) shows that, in terms of atomic-like orbitals, there is a complex hybridization involving many states. The expected Cu-d_{xy} and

O-p states are present, as well as Cu-d_{z^2} and Ti-d states. The Ti ion is surrounded by 6 O ions, three polarized up and three down. Being neighbored by equal numbers of up and down spins, the filled Ti-d orbitals remain unpolarized. The non-negligible amount of Ti-d character in the magnetic bands contradicts the simple formal valency picture and suggests that magnetic interactions may proceed through a path involving non-magnetic Ti orbitals.

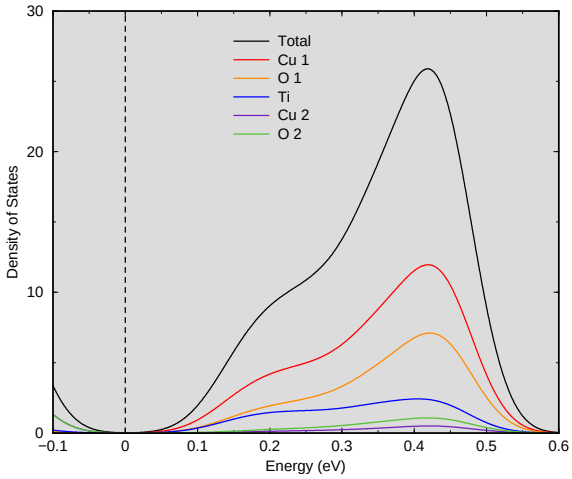

Figure 6.4: Orbitally resolved density of states for the upper (unfilled) magnetic bands of CCTO. Cu, O, and Ti are all non-trivially involved in these bands. The unfilled states are not strictly of one Cu type - both Cu1 and Cu2 characters are present, though the latter is rather small. The origin of these bands is evidently not traceable to a few atomic-like orbitals.

6.3 Model Hamiltonians

A model Hamiltonian differs from a first principles calculation in that it generally neglects certain interactions in favor of others, and often employs parameters that are not calculated but are rather fit to suit the needs of the model. When the complexity of a system is simplified to a few important interactions, there is always information lost, but the trade-off is that a more intuitive and understandable picture results. There are many common

model Hamiltonians being used for a wide variety of systems, and several of these are useful in dealing with the magnetic interactions in CCTO. Beginning with the full Hamiltonian without approximation, we will show which terms are neglected in these models and the names associated with the reduced Hamiltonians in each case.

The full Hamiltonian of a system can be written:

$$\begin{aligned} H =& H_0 + V_{ee} - v^{eff}[\vec{x}_i, \rho] \\ \text{where} \qquad & H_0 = -\frac{h^2}{2m}\nabla^2 + V_{ion}(\vec{x}) + v^{eff}[\vec{x}_i, \rho] \end{aligned} \tag{6.1}$$

H_0 is a single particle Hamiltonian which produces Fock states as eigenstates. The effective potential, v^{eff}, incorporates some of the electron-electron interaction into the single particle part of the Hamiltonian by treating the effects of all the individual electron interactions as an average field in which the single particle moves. V_{ee} includes *all* electron-electron interactions, so the averaged effect of electron-electron Coulomb interactions already taken into account by H_0, (perhaps as a Hartree term or other mean-field term), must be subtracted off to eliminate double counting. The Hamiltonian can be second quantized using the creation and annihilation operators of *single particle* localized eigenstates:

$$\begin{aligned} H =& -\sum_{<i,j>} t_{\alpha ij}\mathbf{c}^\dagger_{\alpha is}\mathbf{c}_{\alpha js} + \sum_{i,j,k,l\alpha,\beta,\delta,\gamma} U^{\alpha\beta\delta\gamma}_{ijkl}\mathbf{c}^\dagger_{\alpha is}\mathbf{c}^\dagger_{\beta js'}\mathbf{c}_{\delta ks'}\mathbf{c}_{\gamma ls} - \sum_{ij} v^{eff}\mathbf{c}^\dagger_{\alpha is}\mathbf{c}_{\alpha js} \\ t_{\alpha ij} =& \int \phi^{*\alpha}_i(\vec{x})\mathbf{H_0}\phi^\alpha_j(\vec{x})d^3\vec{x} \\ U^{\alpha\beta\delta\gamma}_{ijkl} =& \int \phi^{*\alpha}_i(\vec{x})\phi^{*\beta}_j(\vec{y})\mathbf{v}(\vec{x},\vec{y})\phi^\delta_k(\vec{y})\phi^\gamma_l(\vec{x})d^3\vec{x}\,d^3\vec{y} \end{aligned} \tag{6.2}$$

The single particle localized states are given by the ϕ's contained in the integrals and $\mathbf{v}(\vec{x},\vec{y})$ is the bare Coulomb interaction between electrons. It would be impossible

to solve this Hamiltonian in its full detail and even much simpler models are unsolvable under most circumstances, so it becomes immediately necessary to truncate some of the interactions. The idea is to retain as few terms as possible and still capture the physics of the system under consideration.

6.3.1 Creating an Effective Hamiltonian

Once terms are dropped from the full expression of the Hamiltonian, it becomes H^{eff}, an effective Hamiltonian. In what follows, the effective Hamiltonian will still be written as 'H', always keeping in mind that it no longer contains complete information about the system. The determination of which interactions are relevant or necessary and which may be ignored without loss of crucial information is difficult. There is no single proper way to proceed, and the specific system under consideration must dictate the retention or neglect of terms.

A common simplification occurs when the system of interest can be considered as an effective "one-band" model, i.e. $\alpha = \beta = \delta = \gamma$. Ignoring the existence of most of the bands neglects effects that the majority of the bands have on the one (or few) in question, choosing "effective" parameters can be regarded as an attempt to compensate for the neglect. Given that it is even possible to cast the system in terms of one band (or one effective band), important physical consequences of the true multi-band system are missing from the description, specifically the screening of the Coulomb interaction. Within the confinements of a simple model H, however, CCTO is an ideal system for a one-band type of simplification. There is no entanglement between the magnetic bands and other bands, so all but the three highest filled bands and the three lowest empty bands can be

disregarded for the description (modeling) of low energy processes.

Another simplification is possible in situations where the U terms are all negligible in comparison to the t term. Then the Hamiltonian only involves the hopping from one orbital to another and no effects from V_{ee} are taken into account. This is known as the Tight-Binding model and will be discussed in detail in section 6.5. For CCTO, it is not at all possible to claim that the U terms are smaller than the t terms and in fact, we will later assert that t << U in order to facilitate the use of another model. Using the tight-binding model for this compound is justified however because our first principles calculation, which employed the LDA, included only 'mean field' U interactions, *i.e.* those Coulomb terms included in H_0 of Eq. 6.1. Some of these interactions are important to the system and will be added later, but the starting point will be a modeling of the LAPW calculation. The best model will include only those terms that the original calculation employed.

If the non-'mean field' U terms cannot be discarded entirely, then the Hamiltonian can be simplified by keeping only the largest of them. U_{ijkl} will be largest when all indices are the same (U_{iiii}) and all U terms with other combinations of indices are often neglected. This leaves a minimal set of interactions known as the Hubbard Model:

$$H = \sum_{<i,j>} t_{ij}\mathbf{c}_i^\dagger \mathbf{c}_j + \sum_i U n_{i\uparrow} n_{i\downarrow}; \qquad < i,j > \text{indicates sum over each set of neighbors} \tag{6.3}$$

Even the extremely simplified Hubbard model is not exactly solvable in general except in one dimension. Under some special circumstances, however, it can be reduced even further. If U >> t_{ij}, and there are half as many electrons in the system as there are orbitals being considered (i.e. the system is at half-filling), then the ground state will

have either $n_{i\uparrow} = 1$, $n_{i\downarrow} = 0$ or vice versa for every site i, with an associated ground state energy of zero. The t_{ij} term can be treated as a perturbation to this approximate ground state. There is no first-order correction, but second order perturbations, along with the identity $\mathbf{S}_i = \frac{1}{2}\sum c_{is}^{\dagger}\vec{\sigma}_{ss'}c_{is'}$ ($\vec{\sigma}_{ss'}$ = vector of Pauli matrices) allow transformation to a Hamiltonian which depends only on spin-spin interactions. This is known as the Heisenberg Hamiltonian:

$$H = \sum_{<i,j>} \underbrace{\frac{4t_{ij}^2}{U}}_{J_{ij}} \mathbf{S}_i \cdot \mathbf{S}_j \tag{6.4}$$

In this formulation, J_{ij} is always positive and the lowest energy will be associated with the anti-alignment of the two spins connected by this parameter. When written this way, J_{ij} is a superexchange (exchange through an intervening ligand) constant which produces an anti-alignment of spins that models anti-ferromagnetic interactions. The limit $U >> t_{ij}$ is valid for the magnetic bands of interest in CCTO. These bands are relatively flat, which is a measure of the localization of the magnetic orbitals and indicates that U is probably large. Furthermore, the dispersion of the bands is fairly weak - the full bandwidth is only ~ 0.5 eV. Although the exact value of U is unavailable from our calculations, a general idea of its magnitude can be obtained by looking at the U calculated in other materials with similarly localized Cu-d bands. In copper oxide planes, the value of U is often between 7 and 9 eV, but the isolated CuO_4 plaquettes of CCTO are more highly screened and a value of around 4 eV is more likely [34]. This value is large enough to legitimize the use of the Heisenberg Hamiltonian.

Any truncation of the full Hamiltonian brings with it a loss of information. The

screening of the bare Coulomb interaction, $\frac{e^2}{\vec{r_1}-\vec{r_2}}$ is an important physical effect that is swept under the rug when these approximations are made. Once the information about screening contained in the exact Hamiltonian has been lost, it is very hard to know how to mimic its effects on the system. In this treatment, we will not make any attempt to do a good or even adequate job of reinstating the effects of screening. The bare Coulomb interaction will be used in the Hamiltonian (see below) and any corrections for screening will be made ad-hoc to calculated parameters.

6.4 Connecting LAPW results with Model Calculations

The t_{ij}'s contained in the H_{ij} matrix elements contain all the information about single particle motion in the external potential and with in effective potential which tries to take into account the interaction of one electron with all the others. Since the first principles calculation of the band structure was done using the same formalism (single particle, effective potential), the tight-binding band structure is expected to be able to reproduce the LAPW band structure very accurately, provided enough terms are kept. The first step toward analyzing the magnetic order of CCTO on an interaction by interaction basis will be to vary the t_{ij}'s (tight-binding parameters) until a good fit to the first principles band structure is achieved. The set of t_{ij}'s that result from the fit will depend on how many interactions are kept. If the full set (every t_{ij} without exception) is kept, the band structure could be reproduced exactly, but varying this number of parameters would be impossible. Therefore, a truncated number of interactions is kept and these are varied to give the best possible fit to the reference band structure. The specific value of each t_{ij} will vary

somewhat as more and more terms are included, but for a given number of terms, the parameters should be uniquely defined by the best fit.

Once a good tight-binding fit has been achieved, the important hopping parameters are known. These can be used to generate the J_{ij}'s of the Heisenberg model. This will provide information about which spins are interacting with what strength and presumably explain the mechanism by which CCTO orders. In addition,the Heisenberg model can be manipulated to give information about low-lying magnetic excitations called spin waves. A calculation of the spin waves of CCTO is carried out in section 6.6. Finally, an extension to the Hubbard model will be employed to take into account some magnetic interactions beyond the superexchange picture which may be important to understand the magnetic structure of CCTO more fully. This extension will involve the direct exchange term of the Hamiltonian and is also discussed in the spin waves section.

6.5 Tight-Binding Model

The tight-binding model provides an alternative way of deriving the band structure. This model assumes that the real eigenfunctions of an extended crystal can be expressed as a linear combination of single-particle orbitals localized at each site:

$$\psi_{\vec{k}}(\vec{r}) = \frac{1}{\sqrt{N}} \sum_{i,\vec{R}} a_i(\vec{k}) \phi_i(\vec{r} - \vec{R}) e^{i\vec{k}\cdot\vec{r}} \tag{6.5}$$

In order to satisfy Bloch's theorem, each localized orbital, $\phi_i(\vec{r} - \vec{R})$, is multiplied by $e^{i\vec{k}\cdot\vec{R}}$ such that any translation from one site to another through a direct lattice vector leaves the overall wave function unchanged aside from a phase factor. Because the orbitals

used for the expansion are commonly taken to be atomic functions, this method is sometimes called Linear Combination of Atomic Orbitals (LCAO). In this treatment, we will not use atomic orbitals, but the formalism of the model does not depend on the exact form of the basis.

The matrix formulation of the one-electron Schrodinger equation results in the eigenvalue equation:

$$\sum_i [H_{ij}(\vec{k}) - \epsilon_{\vec{k}}\, S_{ij}(\vec{k})] a_i(\vec{k}) = 0 \tag{6.6}$$

$$\text{where} \quad H_{ij}(\vec{k}) = \sum_{\vec{R}} e^{i\vec{k}\cdot\vec{R}} \underbrace{\int \phi_i^*(\vec{r}) H \phi_j(\vec{r} - \vec{R}) d^3\vec{r}}_{t_{ij}}$$

$$\text{and} \quad S_{ij}(\vec{k}) = \sum_{\vec{R}} e^{i\vec{k}\cdot\vec{R}} \int \phi_i^*(\vec{r}) \phi_j(\vec{r} - \vec{R})$$

When atomic orbitals are used for the ϕ_m, the overlap matrix, S_{ij} is not necessarily diagonal because atomic orbitals on different sites have non-zero overlap, though orbitals are orthogonal to one another on the same site. If a set of basis functions which are orthonormalized are used, or if the overlap matrix is considered to be negligible, then diagonalizing H_{ij} yields the band structure, $\epsilon_n(\vec{k})$.

Calculating the t_{ij} exactly is generally a difficult task (unless a local orbital basis is used for the band calculation) and these parameters are usually fit to a known band structure [35]. Keeping all orbitals on all sites would reproduce the Bloch functions of the first principles calculation, but this is a prohibitively large calculation since the dimension of the matrix to be diagonalized is determined by the number of orbitals that are kept. If

many atomic orbitals participate in the important bands, the number of parameters to vary will be large and a good fit will be difficult to obtain. In CCTO, a complex interaction between many atomic-like orbitals (see Fig. 6.4 is what produces the magnetic bands.

Since we are interested in the magnetism of this compound, only the magnetic bands are of any interest. A simplification of the band structure is possible for use with the tight-binding model in CCTO. Because it is a simple anti-ferromagnet, there are not really 6 distinct magnetic bands present in the system. The Cu1 up bands (Cu1 is defined as the Cu ion with majority spin up) are equal to the Cu2 dn bands (Cu2 is the Cu ion with majority spin down) and vice-versa. Therefore, it is sufficient to look at only the three bands of the paramagnetic case, assuming that the exchange interaction will rigidly shift the on-site energies without changing the t_{ij}'s, leaving the shape of the bands intact. An orbitally projected density of states for CCTO shows that the magnetic bands contain contributions from quite a few atomic-like orbitals. Taking all of these orbitals into account would create a rather large matrix and could result in too large a number of parameters to vary. A better technique is to think of the localized orbital expansion in terms of Wannier functions. A Wannier function can be written in terms of Bloch functions as:

$$\phi_n(\vec{r}-\vec{R}) = \frac{1}{N}\sum_{n'} Q_{nn'}(\vec{k}) \sum_{\vec{k}} e^{-i\vec{k}\cdot\vec{R}} \psi_{nn'\vec{k}}(\vec{r}) \tag{6.7}$$

v The summation over $\vec{k}$ transforms the extended Bloch functions into a localized orbital, centered at $\vec{R}$. Each term is multiplied by an arbitrary phase factor (the unitary matrix $Q_{nn'}(\vec{k})$) which depends only on the crystal momentum and not on position. It can easily be shown that Wannier functions are rigorously orthogonal to one another on different sites:

$$\int \phi_m(\vec{r}-\vec{R})\phi_n(\vec{r}-\vec{R}')d^3\vec{r} = \delta_{RR'}\delta_{mn} \tag{6.8}$$

When Wannier functions are used in place of atomic orbitals, neglecting the overlap in the tight-binding model no longer constitutes an approximation, $S_{ij}(\vec{k}) \rightarrow \delta_{ij}$. The Wannier functions also have the advantage that the number of functions needed to reproduce the bandstructure is exactly equal to the number of bands of interest. Instead of trying to model our Bloch functions by projecting onto atomic orbitals and therefore keeping a large number, we can sum the Bloch functions (with respect to $\vec{k}$) and end up with a single localized orbital for each band. In the case of CCTO, this means that the dimension of the matrix will be reduced to three, one Wannier function for each of the copper sites contained in the unit cell. Now the matrix is small enough even to diagonalize analytically, which allows not only computational ease, but also additional insight.

The Wannier functions are not uniquely defined since each term can be multiplied by any phase factor which depends only on $\vec{k}$ (the $Q_{nn'}(\vec{k})$ term in Eq. 6.7), leaving the charge density (the physical observable) unchanged. Various schemes for selecting these phase factors have been suggested. One which is particularly useful in our case is to use the phase factors to force the symmetry of the Wannier orbital to match the site symmetry of the Cu site to which it is attached. The Cu ions of CCTO sit at a site of mmm symmetry. Each Wannier function will therefore have d_{xy}-like symmetry in the local coordinate system where the x and y axes point along the crystal axes, *i.e.*. the line joining Ca ions which bisects the Cu-O plaquette forms the x-axis). This symmetry property can be used to eliminate some hopping parameters entirely. Moving from an atomic orbital picture to a

Wannier function picture is just a shift in conception which facilitates the use of the tight-binding model. The exact form of the Wannier functions are not necessary in order to make a correspondence between this model and the LAPW band structure. However, the resulting t_{ij}'s contain much information about the extent of the Wannier functions.

6.5.1 Slater and Koster Matrix Elements

The hopping parameter can be estimated in a very general way using the Slater and Koster [36] (SK) matrix elements which express $< \alpha|H_0|\beta >$ in terms of the direction cosines of the vector connecting state β to state α, and some parameters which depend only on the distance between the center of the two orbitals. The direction cosines are just the projections of the unit vector which points from one site to another onto each of the three orthogonal axes. The same axes which are used to define the symmetry of the orbital (xy, xz, or yz in this case) must be used to determine the direction cosines. Taking a Wannier orbital of xy symmetry as a reference point, the SK matrix elements of all neighbors can be calculated using the following three expressions:

$$\begin{aligned} E_{xy,xy} &= 3l^2m^2V_{dd\sigma} + (l^2 + m^2 - 4l^2m^2)V_{dd\pi} + (n^2 + l^2m^2)V_{dd\delta} \\ E_{xy,yz} &= 3lm^2nV_{dd\sigma} + ln(1 - 4m^2)V_{dd\pi} + ln(m^2 - 1)V_{dd\delta} \\ E_{xy,zx} &= 3l^2mnV_{dd\sigma} + mn(1 - 4l^2)V_{dd\pi} + mn(l^2 - 1)V_{dd\delta} \end{aligned} \tag{6.9}$$

The $V_{dd\alpha}, \alpha = \sigma, \pi, \delta$, parameters label different types of orbital overlap. A σ overlap occurs when there is no angular momentum of either orbital around the axis which connects two

sites. Similarly, π and δ overlaps correspond to one and two units of angular momentum around the connecting vector. While the $V_{dd\_}$ parameters will not be useful for our purposes, the Slater-Koster expressions can be used to determine if the overlap of any two orbitals is strictly zero by symmetry.

The 1^{st} Cu neighbors of any given Cu ion are located in the (100) direction and since they are on different sublattices, their orbitals are oriented perpendicularly. The vector connecting any two of these orbitals has direction cosines: l = 0, m = 0, and n = 1.

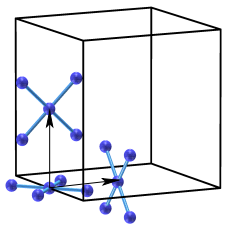

$$E_{xy,yz} = 0 \qquad E_{xy,zx} = 0$$

The inter-sublattice SK matrix elements are zero for this set of l,m,n, indicating that no hopping parameter, t_{ij}, exists between these two orbitals. Since t_{ij} is zero, the superexchange J_{ij} ($= \frac{4t_{ij}^2}{U}$) derived from it is also zero. The lack of superexchange coupling between 1^{st} neighbors means that the anti-alignment between adjacent spins is *not* caused by interaction between these spins themselves, but must be caused by a more complicated set of interactions between more distant neighbors (or by a more complicated model Hamiltonian).

For the 2^{nd} neighbors, the direction cosines are $l = \frac{1}{\sqrt{2}}$, $m = \frac{1}{\sqrt{2}}$, $n = 0$. These orbitals also lie on different sublattices.

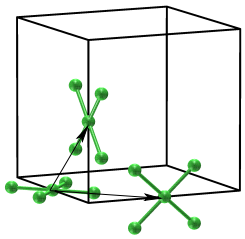

$E_{xy,yz} = 0 \qquad E_{xy,zx} = 0$

Remarkably, the SK matrix elements between all 2^{nd} nearest Cu neighbors, like those of 1^{st} neighbors, are also zero by symmetry. The magnetic ordering must therefore come from even farther away. The next Cu site is the third neighbor which lies in the (111) direction and belongs to the same sublattice. The direction cosines are l = $\frac{1}{\sqrt{3}}$, m = $\frac{1}{\sqrt{3}}$ n = $\frac{1}{\sqrt{3}}$.

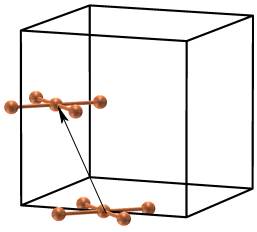

$E_{xy,xy} \neq 0$

The SK matrix element between 3^{rd} Cu neighbors is non-zero, indicating that J_3 is present. This intra-sublattice interaction can however *only order each sublattice with respect to itself.* The interaction is antiferromagnetic and therefore corresponds correctly to the experimentally observed order, but it provides no mechanism by which the sublattices can order with respect to one another. Ordering through 3^{rd} neighbors produces three separately (and correctly) aligned sublattices but does not produce the Néel order that is observed.

All 4^{th} neighbors lie on a single sublattice with direction cosines l = 1, m = 0 , n = 0.

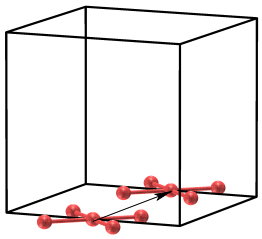

$E_{xy,xy} \neq 0$

The SK matrix element between like orbitals is non-zero, yielding a non-zero J_4 as well. This interaction suffers the same deficiency as J_3: it does not connect different sublattices. Additionally, the anti-alignment of 4^{th} neighbors which J_4 promotes is disruptive to the observed AFM order of the crystal. This interaction not only does not explain the ordering that is seen, but it is frustrating (favors alignment which is counter to the alignment encouraged by other present interactions) and must be overcome by other couplings if the observed magnetic order is to result from the model.

The 5^{th} neighbor coupling is non-zero and occurs between spins which are not located on the same sublattice. 5^{th} neighbors are widely separated and have direction cosines $l = \frac{1}{\sqrt{6}}$, $m = \frac{1}{\sqrt{6}}$, $n = \sqrt{\frac{2}{3}}$.

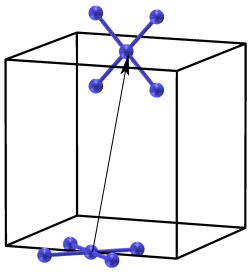

$E_{xy,yz} \neq 0 \qquad E_{xy,xz} \neq 0$

This is the first superexchange coupling which could conceivably order the entire lattice. It connects Cu sites which are separated from one another by more than a full lattice constant ($d_{5^{th}} = \sqrt{\frac{5}{4}}a \approx 9\mathring{A}$). If 5^{th} neighbors are anti-aligned and the sublattices are antiferromagnetically ordered, the full crystal will have the simple Néel order that is experimentally

observed (finally!).

The simple SK matrix elements reveal that in order to account for the ordering in CCTO in the superexchange picture, J_{ij}'s out to at least 5^{th} Cu neighbors will have to be included. Thus, the tight-binding model should include t_{ij}'s up to at least this distance as well. This means that there are (at least) five tight-binding parameters required. This is a much more manageable number than the set of parameters which would be required in an atomic-like orbital picture where the path between 5^{th} Cu neighbors would be Cu-O-Ti-O-Ti-O-Cu. More terms than five are actually needed even in the Wannier orbital picture, because the paths which connect neighbors at the same distance are not always isotropic. For both 4^{th} and 7^{th} (see below) neighbors, there are several different parameters for one of two reasons. In some cases, the Wannier orbitals involved in these hopping terms are oriented differently with respect to one another (they lie on different sublattices) which produces a different magnitude of hopping. In other cases, the orientation does not change, but the chemical environment is actually different, such that the path from one orbital to another along one direction requires going through a Ca while along a second direction it does not.

The matrix in terms of Wannier orbitals is only 3x3 and can be diagonalized analytically. Diagonalization must be done for each k-point of interest and we choose to use some common high symmetry directions in the primitive Brillouin zone as our sample. Since the paramagnetic band structure of CCTO can be generated using the original bcc lattice (no doubling due to magnetic order is necessary), these k-points correspond to directions in an fcc Brillouin zone.

Using the hopping parameters from only the 3^{rd} and 4^{th} neighbors (recall that 1^{st} and 2^{nd} vanish by symmetry), a reasonable fit to the LAPW band structure is possible. Though the shape is approximately correct, one important degeneracy is left unbroken. Along the Γ - P (111) direction, the true bands are split near the edge of the zone, while the tight-binding bands remain degenerate. The degeneracy in this region is a result of the lack of appropriate coupling between sublattices. Adding the 5^{th} neighbor coupling successfully breaks the degeneracy and the fit becomes even better. However, an excellent fit can be obtained by adding a 7^{th} neighbor coupling term. The 7^{th} neighbor is probably not extremely important to the magnetic order, as it couples spins located on the same sublattice. In fact the 7^{th} neighbor interaction is very similar to the 4^{th} - it generates three separate hopping amplitudes, and it is frustrating to the observed magnetic ordering. Though its importance to the magnetic order seems minor, its inclusion in the tight-binding model results in an extremely close fit. The magnitude of the greatest of the three t_7 parameters is greater than that of the t_5 parameter and could therefore be considered more important in terms of the band structure shape, and therefore perhaps to the superexchange magnetic picture as well.

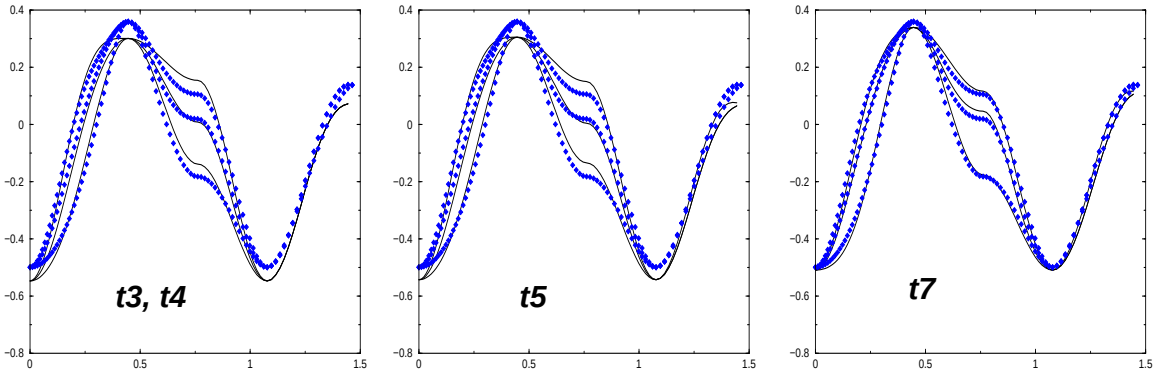

Figure 6.5: Tight-binding fit compared with LAPW band structure. TB model is shown by solid lines while the LAPW bands are diamonds. Important non-degeneracies are not possible without the t_5 interaction (second panel) and a very good fit depends on the inclusion of t_7 (third panel)

The tight-binding parameters which yielded the best fit (shown in the third panel of Fig. 6.5) are enumerated in Table 6.1. The expected anisotropies in 4^{th} and 7^{th} neighbor hoppings turn out to be fairly extreme. Orientation differences are indicated using the common chemical bonding labels and the chemical differences are noted by stating whether or not Ca ions lie along the most direct bonding path.

Table 6.1:

t_{3rd}		-53.0 meV
t_{4th}	π(Ca)	-51.0 meV
$t_{4th'}$	π(no Ca)	16.3 meV
$t_{4th''}$	δ	20.1 meV
t_{5th}		5.6 meV
t_{6th}		-.7 meV
t_{7th}	σ	-1.4 meV
$t_{7th'}$	δ (Ca)	2.7 meV
$t_{7th''}$	δ (no Ca)	-9.5 meV

The tight-binding fit is sufficiently close to the LAPW generated band structure

that any further superexchange interactions of the $\frac{4t^2}{U}$ type can confidently be ignored. Though the 5^{th} neighbor interaction is both small and distant, its inclusion can explain the overall magnetic order. The 7^{th} neighbor coupling, though larger than the 5^{th} couples only spins on the same sublattice and so cannot account for inter-sublattice ordering. Given the magnitudes of the hopping parameters as obtained from the tight-binding fit, the classical Ising AFM state of CCTO is energetically favorable over the FM state. Assuming that $S_x = S_y = 0$, (i.e. $\mathbf{S}_i \cdot \mathbf{S}_j = +/- S^2$), and the fitted t_{ij}'s along with $S = \frac{1}{2}$ and U = 4 eV, the N*éel* order is favored by 23 meV/Cu over the FM order. The specific contributions to the energy are listed in Table 6.2. Because the value of U cannot be determined by the tight-binding fit, we have used what is thought to be a reasonable value, 4 eV, taken from calculations of this parameter in compounds where the Cu ion is in isolated plaquettes, not edge or corner sharing.

Table 6.2:

Type of Hopping		z_{nn}	$\frac{4t^2}{U} * z_{nn}$ (FM)	$\frac{4t^2}{U} * z_{nn}$ (AFM)
t_{3rd}		8	22.47 meV	-22.47 meV
t_{4th}	π(Ca)	2	5.2 meV	5.2 meV
$t_{4th'}$	π(no Ca)	2	0.53 meV	0.53 meV
$t_{4th''}$	δ	2	0.81 meV	0.81 meV
t_{5th}		8	0.25 meV	-0.25 meV
t_{6th}		12	0.00 meV	0.00 meV
t_{7th}	σ	4	0.01 meV	-0.01 meV
$t_{7th'}$	δ (Ca)	4	0.03 meV	-0.03 meV
$t_{7th''}$	δ (no Ca)	4	0.36 meV	-0.36 meV
TOTAL			29.66 meV	-16.58 meV

The simple superexchange model of spin interactions can adequately explain the magnetic order of CCTO, but surprisingly, its success hinges on interactions which occur

between Cu spins which are separated by more than a lattice constant. The inclusion of ferromagnetic or direct exchange couplings between Cu spins may be important to fully understand the magnetic structure of this compound. The effect of these interactions on the magnetic order and on the magnetic excitations of CCTO is investigated in the context of spin waves.

6.6 Spin Waves

In order to investigate magnetic excitations and to compare to neutron scattering and Raman data, we must take into account quantum spin fluctuations which are neglected in the DFT calculation. The starting point is the Heisenberg Hamiltonian and, as before, the J_{ij}'s are obtained from the tight-binding parameters, t_{ij} through the relationship $J_{ij} = \frac{4t_{ij}}{U}$. In this way, accurate information about the ground state, obtained from density functional calculations, is used to gain information about excited states. Written in terms of spin operators, the Heisenberg Hamiltonian is:

$$H = \sum_{<i,j>} J_{ij}[\frac{1}{2}(S_i^+ S_j^- + S_i^- S_j^+) + S_i^z S_j^z] \tag{6.10}$$

The Holstein-Primakoff transformation [37] is used to map the spin operators onto a set of boson operators:

$$\begin{aligned} \mathbf{S_j^+} &= (2S)^{\frac{1}{2}}(1 - a_j^\dagger a_j 2S)^{\frac{1}{2}}\mathbf{a_j} \\ \mathbf{S_j^-} &= (2S)^{\frac{1}{2}}\mathbf{a_j}^\dagger(1 - a_j^\dagger a_j/2S)^{\frac{1}{2}} \\ \mathbf{S_j^z} &= S - \mathbf{a_j}^\dagger\mathbf{a_j} \end{aligned} \tag{6.11}$$

The final expression follows from $S_z = (S(S+1) - S_x^2 - S_y^2)^{\frac{1}{2}}$ with substitution of the HP operator expressions for the spin operators S_x and S_y. If $\mathbf{a}^\dagger$ and $\mathbf{a}$ follow the standard

bosonic commutation relations [$\mathbf{a_j^\dagger}$,$\mathbf{a_k}$] = δ_{jk} , then the proper commutation relations for the spin operators will be preserved.

Taking the sum over j of the expression for S_z gives S^z_{TOT} = NS - $\sum_j \mathbf{a_j}^\dagger\mathbf{a}$. In the absence of HP bosons, the total spin in the z-direction is just the total number of spins multiplied by the magnitude of one spin, i.e. each spin is fully aligned along the axis of quantization. Each boson present in the system decreases this total spin by one, yielding the interpretation that, for a spin $\frac{1}{2}$ system, each HP boson operator flips a single spin:

$$\mathbf{a_i^\dagger}|\uparrow_1\uparrow_2 ... \uparrow_i\uparrow_{i+1} ...\rangle = |\uparrow_1\uparrow_2 ... \downarrow_i\uparrow_{i+1} ...\rangle$$

But a single flipped spin is not a stable configuration in an extended crystal and the unit decrease in the z-component of the total spin of the system gets distributed throughout the system, tilting each spin such that the z-component is decreased by 1/N (where N is the total number of spins on the lattice under consideration). The spins precess around the z-axis, each with the same frequency. The energy of each magnon is determined by the phase relationship between adjacent spins, and the phase relationship is determined by the wave vector $\vec{k}$ of the spin wave.

Figure 6.6: FM spin wave: all spins are originally aligned along the z-axis and subsequently tilted by the presence of a magnon. Precession frequency is determined by the ω vs. $\vec{k}$ dispersion relation. In this figure, the phase difference is $\approx \frac{2\pi}{5}$.

This situation is well-described by a Fourier transform of the HP boson operators into magnon operators. Each Fourier-transformed operator creates or annihilates a spin

wave, or a magnon, of wave vector $\vec{k}$.

$$\begin{aligned} \mathbf{a}_{\mathbf{k}}^{\dagger} &= \frac{1}{\sqrt{N}} \sum_{j} e^{-i\vec{k}\cdot\vec{x}_j} \mathbf{a}_{\mathbf{j}}^{\dagger} \\ \mathbf{a}_{\mathbf{k}} &= \frac{1}{\sqrt{N}} \sum_{j} e^{i\vec{k}\cdot\vec{x}_j} \mathbf{a}_{\mathbf{j}} \end{aligned} \tag{6.12}$$

Whereas a single spin flip costs zJ in energy (z = # of nearest neighbors), a magnon may have a much smaller exchange energy.

When there are multiple magnetic sites per unit cell, separate operators for each site must be created. $\vec{k}$ then labels the phase relationship between one type of spin and its equivalent in the next unit cell. The specific phase relationship between spins located within the same unit cell will contribute to the energy of the magnon.

In this model, spin waves are a perturbation around a known (or presumed) magnetic ground state. If the ground state is ferromagnetic, then the z-components of all spins remain aligned as in the cartoon above. If the system is anti-ferromagnetic, the z-components of adjacent spins will be anti-aligned and the precession of spins with z-component 'up' will be in the opposite direction of those pointing 'down'. Therefore, in an antiferromagnetic situation, it is necessary to subdivide the lattice into two sub-lattices, one carrying only up spins (the a sublattice) and one carrying only down spins (the b sublattice). There are separate spin operators for each sublattice, reflecting the fact that the spin raising and lowering operators act differently on a spin pointing along the z-axis than on a spin pointing along the negative z-axis.

If the model is constrained to investigate only low-lying excitations, then it is valid to assume that $\langle a_k^{\dagger} a_k \rangle \ll 2S$ and expand the square root contained in the spin operator

transformation, Eq. 6.12 Substituting the expression for the magnon operators into this expanded definition gives for separate a and b sublattices:

$$\begin{aligned}
\mathbf{S}^{+}_{\mathbf{aj}} &= (2S/N)^{\frac{1}{2}} \sum_{\vec{k}} \left[e^{-i\vec{k}\cdot\vec{x}_j} \mathbf{a_k} + ... \right] \qquad & \mathbf{S}^{-}_{\mathbf{aj}} &= (2S/N)^{\frac{1}{2}} \sum_{\vec{k}} \left[e^{i\vec{k}\cdot\vec{x}_j} \mathbf{a}^{\dagger}_{\mathbf{k}} + ... \right] \\
\mathbf{S}^{+}_{\mathbf{bj}} &= (2S/N)^{\frac{1}{2}} \sum_{\vec{k}} \left[e^{-i\vec{k}\cdot\vec{x}_j} \mathbf{b}^{\dagger}_{\mathbf{k}} + ... \right] \qquad & \mathbf{S}^{-}_{\mathbf{bj}} &= (2S/N)^{\frac{1}{2}} \sum_{\vec{k}} \left[e^{i\vec{k}\cdot\vec{x}_j} \mathbf{b_k} + ... \right] \\
\mathbf{S}^{\mathbf{a}}_{\mathbf{jz}} &= S - \frac{1}{N} \sum_{\vec{k}} e^{i(\vec{k}-\vec{k}')\cdot\vec{x}_j} \mathbf{c}^{\dagger}_{\mathbf{k}} \mathbf{c_k} \qquad & \mathbf{S}^{\mathbf{b}}_{\mathbf{jz}} &= S - \frac{1}{N} \sum_{\vec{k}} e^{-i(\vec{k}-\vec{k}')\cdot\vec{x}_j} \mathbf{b}^{\dagger}_{\mathbf{k}} \mathbf{b_k}
\end{aligned} \tag{6.13}$$

The final expression for the spin wave Hamiltonian is obtained by the insertion of these operators into the original Heisenberg Hamiltonian. The linear spin wave approximation keeps only terms that are bilinear in magnon operators. The neglected terms represent magnon-magnon interactions and are presumed to be absent in the low-lying states under investigation.

In order to calculate the spin waves for CCTO, it is first necessary to divide it into three bcc sublattices, A,B,C, corresponding to the three spin sites per unit cell. A given sublattice is made up of Cu ions whose unpaired spin sits in one of the three t_{2g} states, with plaquette orientations of either xy, yz, or xz.

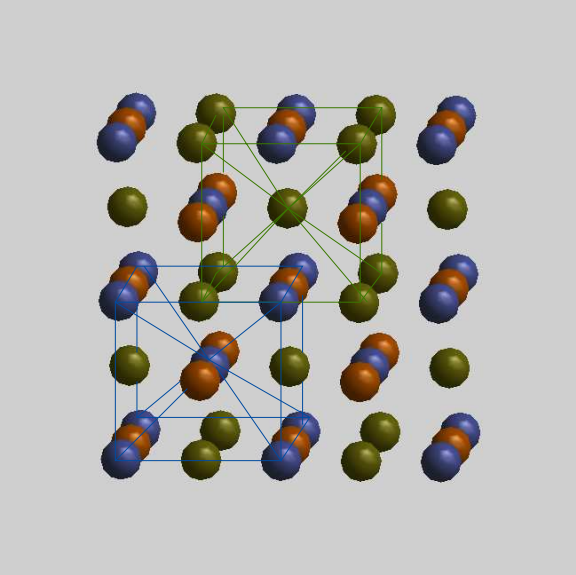

Figure 6.7: The CCTO lattice with only Cu positions shown. Each color corresponds to a bcc sublattice which contains Cu-O plaquettes in a specific orientation - lines connecting each separate sublattice to itself emphasize the bcc structure. The overall bcc structure of the full compound is achieved by the interleaving of the three separate bcc sublattices

Each of the three bcc sublattices is further divided into two inter-penetrating simple cubic sub-sublattices, a and b as mentioned above, corresponding to the spin orientation with respect to the z-axis. The partition of the CCTO structure into 3 sublattices each with two sub-sublattices each results in the set of six HP operators (and their Hermitian conjugates) needed to write out the Hamiltonian for this compound. The six operators are labeled by sublattice and spin direction (indicated by sub-sublattice a or b):

$$\mathbf{Aa}^\dagger, \mathbf{Ab}^\dagger, \mathbf{Ba}^\dagger, \mathbf{Bb}^\dagger, \mathbf{Ca}^\dagger, \mathbf{Cb}^\dagger$$

Considering superexchange interactions only, the first non-zero coupling is J_3. This term couples spins which are on the same sublattice, but different sub-sublattices. A given spin will have z neighbors, each connected by a vector $\vec{\delta}$. Using the proper operator expres-

sions for each sub-sublattice, the term in the Hamiltonian which corresponds to third Cu neighbor interactions is (neglecting $\vec{k}$-independent constants):

$$\begin{aligned} H_3 = J_3 S z_3 [\sum_{\vec{k}} \gamma_{\vec{k}} (& \mathbf{A}\mathbf{a}_{\vec{k}} \mathbf{A}\mathbf{b}_{\vec{k}} + \mathbf{A}\mathbf{a}^{\dagger}_{\vec{k}} \mathbf{A}\mathbf{b}^{\dagger}_{\vec{k}} + \mathbf{B}\mathbf{a}_{\vec{k}} \mathbf{B}\mathbf{b}_{\vec{k}} + \mathbf{B}\mathbf{a}^{\dagger}_{\vec{k}} \mathbf{B}\mathbf{b}^{\dagger}_{\vec{k}} + \mathbf{C}\mathbf{a}_{\vec{k}} \mathbf{C}\mathbf{b}_{\vec{k}} + \mathbf{C}\mathbf{a}^{\dagger}_{\vec{k}} \mathbf{C}\mathbf{b}^{\dagger}_{\vec{k}}) \\ & + \mathbf{A}\mathbf{a}^{\dagger}_{\vec{k}} \mathbf{A}\mathbf{a}_{\vec{k}} + \mathbf{B}\mathbf{a}^{\dagger}_{\vec{k}} \mathbf{B}\mathbf{a}_{\vec{k}} + \mathbf{C}\mathbf{a}^{\dagger}_{\vec{k}} \mathbf{C}\mathbf{a}_{\vec{k}}] \\ \gamma_{\vec{k}} = & \frac{1}{z} \sum_{\vec{\delta}} e^{i\vec{k}\cdot\vec{\delta}}; \qquad z = \#\text{ of neighbors}; \qquad \vec{\delta} \text{ connects neighbors} \end{aligned} \tag{6.14}$$

This Hamiltonian can be diagonalized by making a linear combination of the magnon operators. The new transformed operators lack the simple interpretation of the magnon operators (each creates a magnon of a given $\vec{k}$ on a given sub-sublattice) because they mix creation and annihilation operators together, as well as mixing operators which belong to different sub-sublattices. However, the new operators do not mix magnons of different wave vectors, so the phase relationship between unit cells is preserved. The specific combination of operators which diagonalizes this matrix is the same used in the well-known case of superconductivity (BCS) and goes by the name of the Bogoliubov [38] transformation:

$$\boldsymbol{\alpha}_{\vec{k}} = u_{\vec{k}} \mathbf{a}_{\vec{k}} - v_{\vec{k}} \mathbf{b}^{\dagger}{}_{\vec{k}} \qquad \boldsymbol{\beta}_{\vec{k}} = u_{\vec{k}} \mathbf{b}_{\vec{k}} - v_{\vec{k}} \mathbf{a}^{\dagger}{}_{\vec{k}} \tag{6.15}$$

Taking the inverse of these equations yields expressions for the original magnon operators which are substituted into the Hamiltonian from which the dispersion relation can now easily be extracted:

$$\begin{aligned} H = & \sum_{\vec{k}} \epsilon_{\vec{k}} (\boldsymbol{\alpha}^{\dagger}_{\vec{k}} \boldsymbol{\alpha}_{\vec{k}} + \boldsymbol{\beta}^{\dagger}_{\vec{k}} \boldsymbol{\beta}_{\vec{k}}) \\ \epsilon_{\vec{k}} = & 2Jsz_3 (1 - \gamma^2_{\vec{k}})^{\frac{1}{2}} \end{aligned} \tag{6.16}$$

In crystals where inversion symmetry is present (which is the case for CCTO), each $\vec{\delta}$ will enter the sum in Eq. 6.14 accompanied by a - $\vec{\delta}$ and therefore $\gamma_{\vec{k}} \sim \cos(k)$. So the dispersion for the third neighbor interaction goes like sin(k). This linear dispersion away from the Γ point is characteristic of AFM magnons.

The next non-zero coupling between Cu sites is J_4. This term couples spins on the same sublattice as well as the same sub-sublattice, *i.e.* both spins lie on orbitals of the same orientation and in the presumed ground state, have the same direction. Because these spins are aligned with one another in the ground state, the term in the spin wave Hamiltonian which corresponds to their interaction is identical to the expression derived for a ferromagnetic, simple cubic lattice. It is already diagonal in the magnon operators, so that no further operator transformation is needed in order to obtain the dispersion relation:

$$H_3 = J_4 s z_4 \sum_{\vec{k}} (\gamma_{\vec{k}} - 1)\{\mathbf{A}\mathbf{a}^{\dagger}_{\vec{k}}\mathbf{A}\mathbf{a}_{\vec{k}} + \mathbf{B}\mathbf{a}^{\dagger}_{\vec{k}}\mathbf{B}\mathbf{a}_{\vec{k}} + \mathbf{C}\mathbf{a}^{\dagger}_{\vec{k}}\mathbf{C}\mathbf{a}_{\vec{k}}\} \tag{6.17}$$

From this expression, it is clear that the FM dispersion differs from the AFM dispersion. As before, $\gamma_{\vec{k}} \sim \cos(k)$, such that in the long wavelength limit, $\epsilon_{\vec{k}} \sim k^2$. Near the Γ point, the dispersion is quadratic, in contrast to the linear dispersion seen in the AFM regime.

The 4^{th} neighbors sit on a simple cubic lattice, while the 3^{rd} neighbors sit on a bcc lattice. The specific lattice does not affect the shape of the dispersion around the Γ point, but the spectrum away from this point will depend on the location of spins relative to one another. The main differences between FM and AFM spin waves can be seen by including only 3^{rd} neighbors (AFM) or only 4^{th} neighbors (FM)

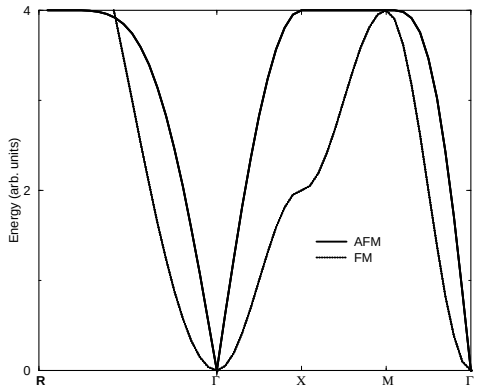

Figure 6.8: A comparison of FM and AFM magnons. The FM magnon is on a simple cubic lattice, the AFM magnon is on a bcc lattice. These two specific lattices are chosen to represent the 3^{rd} and 4^{th} neighbor lattices of CCTO respectively. 4^{th} neighbors are all aligned and, in the absence of other interactions, the 4^{th}-neighbor-only simple cubic sublattice supports FM magnons. 3^{rd} neighbors are anti-aligned and AFM magnons propagate through the bcc lattice composed of these neighbors. The 3^{rd} neighbor lattice here is one of the three sublattices pictured in Fig. 6.7.

In reality, the J_4 interaction in CCTO is anisotropic, so this term must be split into three different terms, each identical except for its respective J and $\gamma_{\vec{k}}$:

$$J_4 \Longrightarrow \sum_i J_{4i},\ \gamma_{\vec{k}} \Longrightarrow \sum_i \gamma_{\vec{k}i}; \qquad \text{i indexes } \pi(Ca),\ \pi(noCa),\ \delta$$

The dispersion remains linear but this formulation splits the bands in some symmetry directions, along which they would otherwise be degenerate, which is a manifestation of symmetry breaking.

Both of the terms just derived (3rd and 4th neighbor interactions) must be included simultaneously in the Hamiltonian for CCTO. The Bogoliubov transformation, which is necessary to diagonalize the 3rd neighbor terms, has the fortunate property that it does not disturb terms which are already diagonal in the original magnon operators. Therefore, making a Bogoliubov transformation of all the operators will result in a fully diagonal

Hamiltonian. If only 3rd and 4th Cu neighbor interactions were to be considered, this result would be sufficient. But in the superexchange picture, it is the small interaction between 5th neighbors which renders the lattice fully connected. Without it, the three sublattices act independently. Magnons which do not take into account this interaction will be triply degenerate. The non-interaction between sublattices eliminates the possibility of optical magnons which arise from the energy associated with spins within a single unit cell rotating against one another.

The term which is derived from the 5th Cu neighbor interaction connects each sublattice to both of the others. All 5th Cu neighbors are anti-aligned, so the operators come from opposite sub-sublattices (a connects to b and vice-versa):

$$\begin{aligned} H_5 = J_5 s z_5 [\sum_{\vec{k}} & \gamma_{\vec{k}AB} (\mathbf{Aa}_{\vec{k}} \mathbf{Bb}_{\vec{k}} + \mathbf{Aa}^\dagger_{\vec{k}} \mathbf{Bb}^\dagger_{\vec{k}} + \mathbf{Ab}_{\vec{k}} \mathbf{Ba}_{\vec{k}} + \mathbf{Ab}^\dagger_{\vec{k}} \mathbf{Ba}^\dagger_{\vec{k}}) \\ & + \gamma_{\vec{k}AC} (\mathbf{Aa}_{\vec{k}} \mathbf{Cb}_{\vec{k}} + \mathbf{Aa}^\dagger_{\vec{k}} \mathbf{Cb}^\dagger_{\vec{k}} + \mathbf{Ab}_{\vec{k}} \mathbf{Ca}_{\vec{k}} + \mathbf{Ab}^\dagger_{\vec{k}} \mathbf{Ba}^\dagger_{\vec{k}} \\ & + \gamma_{\vec{k}BC} (\mathbf{Ba}_{\vec{k}} \mathbf{Cb}_{\vec{k}} + \mathbf{Ba}^\dagger_{\vec{k}} \mathbf{Cb}^\dagger_{\vec{k}} + \mathbf{Bb}_{\vec{k}} \mathbf{Ca}_{\vec{k}} + \mathbf{Bb}^\dagger_{\vec{k}} \mathbf{Ca}^\dagger_{\vec{k}}) \\ & - 2 (\mathbf{Aa}^\dagger_{\vec{k}} \mathbf{Aa}_{\vec{k}} + \mathbf{Ba}^\dagger_{\vec{k}} \mathbf{Ba}_{\vec{k}} + \mathbf{Ca}^\dagger_{\vec{k}} \mathbf{Ca}_{\vec{k}} + \mathbf{Ab}^\dagger_{\vec{k}} \mathbf{Ab}_{\vec{k}} + \mathbf{Bb}^\dagger_{\vec{k}} \mathbf{Bb}_{\vec{k}} + \mathbf{Cb}^\dagger_{\vec{k}} \mathbf{Cb}_{\vec{k}}) \end{aligned} \tag{6.18}$$

Unlike the previous two terms, this will not be diagonalized by a simple Bogoliubov transformation. However, a linear combination of operators that does diagonalize the matrix can be found, using a fairly simple methodology. If $\boldsymbol{\alpha}_{\vec{k}}$ (and its Hermitian conjugate) are the operators which successfully diagonalize the Hamiltonian, then:

$$H = \sum_{\vec{k}} \epsilon_{\vec{k}} (\boldsymbol{\alpha}^\dagger_{\vec{k}} \boldsymbol{\alpha}_{\vec{k}}); \qquad \text{so that} \qquad [H, \boldsymbol{\alpha}_{\vec{k}}] = \epsilon_{\vec{k}} \boldsymbol{\alpha}_{\vec{k}}. \tag{6.19}$$

There are twelve total possible magnon operators (creation and annihilation). Six of these form a set in which the commutator of one of them with the Hamiltonian produces terms which contain only the others. The remaining six operators form another set with the same properties. From this it is clear that any linear combination of operators that follows the above commutation expression must be comprised of all six of these operators and no others. This operator will create the magnon normal modes. It is formulated as follows:

$$\boldsymbol{\alpha}_{\vec{k}} = u_{\vec{k}}\mathbf{A}\mathbf{a}_{\vec{k}} + v_{\vec{k}}\mathbf{B}\mathbf{a}_{\vec{k}} + w_{\vec{k}}\mathbf{C}\mathbf{a}_{\vec{k}} + x_{\vec{k}}\mathbf{A}\mathbf{b}^{\dagger}_{\vec{k}} + y_{\vec{k}}\mathbf{B}\mathbf{b}^{\dagger}_{\vec{k}} + z_{\vec{k}}\mathbf{C}\mathbf{b}^{\dagger}_{\vec{k}} \tag{6.20}$$

To determine the expansion coefficients ($u_{\vec{k}}$,...., $z_{\vec{k}}$), and thereby establish the normal modes and dispersion relation, Eq. 6.19 is used. The left-hand side of the equation involves taking the commutator of the Hamiltonian with each magnon operator. As stated before, this will produce an expression involving only the operators which comprise $\boldsymbol{\alpha}_{\vec{k}}$. The right side will contain these operators as well, each multiplied by an expansion coefficient and by $\epsilon_{\vec{k}}$. The equation must be satisfied separately for each operator, so the coefficients on each side of the equation are set equal to one another for each of the six operators. This results in a matrix equation for the linear expansion coefficients. The eigenvalues of the matrix are the $\epsilon_{\vec{k}}$.

The following definitions are used to simplify notation:

$$\begin{aligned} &J_3 sz_3 \equiv C \qquad 2\sum_i J_{4i} sz_{4i}(\gamma_{\vec{k}i} - 1) \equiv D \qquad J_5 sz_5 \equiv E \\ &C + D - 2E \equiv P_1 \\ &E\gamma^{AB}_{5\vec{k}} \equiv P_2 \qquad E\gamma^{AC}_{5\vec{k}} \equiv P_3 \qquad E\gamma^{BC}_{5\vec{k}} \equiv P_4 \end{aligned} \tag{6.21}$$

The matrix in terms of the newly defined parameters becomes:

$$\begin{bmatrix} P_1 & 0 & 0 & -C\gamma 3_{\vec{k}} & -P_2 & -P_3 \\ 0 & P_1 & 0 & -P_2 & -C\gamma 3_{\vec{k}} & -P_4 \\ 0 & 0 & P_1 & -P_3 & -P_4 & -C\gamma 3_{\vec{k}} \\ C\gamma 3_{\vec{k}} & P_2 & P_3 & -P_1 & 0 & 0 \\ P_2 & C\gamma 3_{\vec{k}} & P_4 & 0 & -P_1 & -B\gamma 2_{\vec{k}BC} \\ P_3 & P_4 & C\gamma 3_{\vec{k}} & 0 & 0 & -P_1 \end{bmatrix} \tag{6.22}$$

This matrix has the symmetry property that H_{ij} = -H_{ji} for $i \neq j$, but it is not Hermitian - since all elements are real, it is anti-Hermitian. Without Hermiticity, there is no guarantee that the eigenvalues will be real. Of course, complex eigenvalues have no physical meaning, so we will be interested in only those values for the J's which generate 6 real eigenvalues for every k-point within the first Brillouin zone. Because the ground state of the compound was assumed to be AFM and the spin waves were assumed to be small perturbations around this state, J values which would produce an FM ground state are not allowed. In a complicated spin system such as CCTO, it is not always clear where the boundary between AFM and FM states are in terms of J values. The solutions to this matrix can clarify the boundary because J values which violate the ground state assumption end up producing non-physical (imaginary) frequencies.

As an example, the 4th Cu neighbors have a superexchange interaction which wants to anti-align them. However, the stronger J_3 superexchange constant anti-aligns all 3rd Cu neighbors which has the side-effect of aligning the 4th Cu neighbors. If J_4 is increased such that the tendency of these neighbors to anti-align overwhelms the stronger

J_3 interaction, the premise that the ground state of the system is AFM becomes invalid and imaginary eigenvalues appear when the Hamiltonian is diagonalized.

Using the J_{ij}'s derived from the tight-binding model, all of the eigenvalues are real, indicating that these values indeed produce an AFM ground state. The eigenvalues for k-points along high symmetry directions in the Brillouin zone can be plotted and the result is a dispersion curve which is linear around Γ, correctly signaling the presence of AFM order. There is only one experimental data point for the magnon spectrum of CCTO. Neutron scattering results show an optical magnon of 7.3 meV at the Γ point. Along with the full calculated spectrum of magnons, this point is indicated as a black dot in Fig. 6.9.

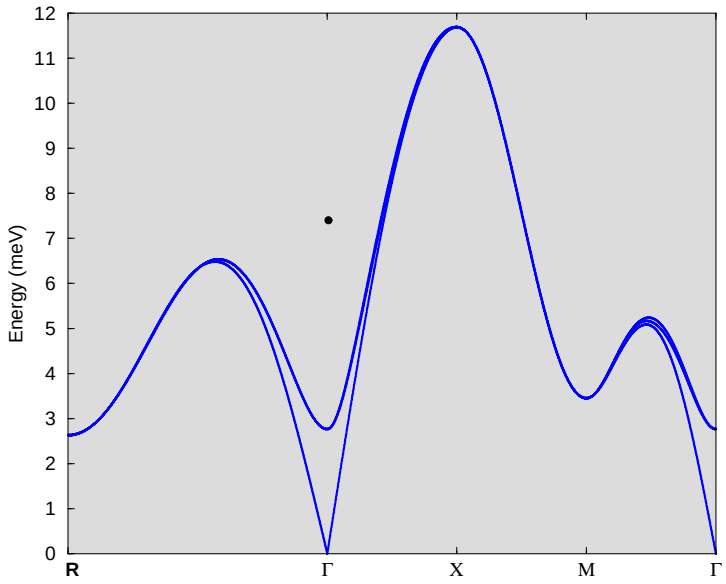

Figure 6.9: The three spin wave branches of CCTO. The 5^{th} neighbor interaction is responsible for all non-degeneracies in the spectrum. The apparent degeneracies along $X - M$ and near R are caused by the very small value of J_5; artificially increasing its value would make the splitting of the bands more obvious.

At the Γ-point, all $\gamma_{\vec{k}}$ factors $\Longrightarrow 1$, and the matrix can be diagonalized analytically, yielding expressions for the frequencies and therefore the energies of the magnons.

There are six solutions - one for each of the original six operators included in the $\alpha_{\vec{k}}$ which diagonalizes the Hamiltonian. However, they are not all independent. The a and b sub-sublattices in each sublattice are forced to have a particular relationship to one another, specifically the spins are anti-aligned. The spins on a given a sub-sublattice precess oppositely to those on the corresponding b sub-sublattice, but the phase relationship between them is fixed. Both the sub-sublattice precession frequencies, which have the same magnitude, emerge as solutions. The Hamiltonian can be divided into blocks:

$$\begin{bmatrix} \tilde{A} & \tilde{B} \\ -\tilde{B} & -\tilde{A} \end{bmatrix}$$ where $\tilde{A}$ and $\tilde{B}$ are each 3 x 3 matrices.

This particular symmetry guarantees that frequency solutions will come in +/- pairs. The forced symmetry of the spin operators which act on a and b sub-sublattices is what gives the Hamiltonian this symmetry. The positive and negative frequencies carry the same energy so these two solutions are energetically degenerate. The expressions for acoustic and optical magnons are given by:

$$\epsilon_0 = 0 \qquad \text{(doubly degenerate)}; \qquad \epsilon_0 = \pm\sqrt{3J_5^2 + 6J_3J_5} \qquad \text{(each doubly degenerate)} \tag{6.23}$$

In order for all the Γ-point magnon energies to be real (physical), the argument of the square root must be positive or $J_5 + 2J_3 > 0$. Since all superexchange constants are positive, this condition is never violated. However, the expression away from the Γ-point becomes more complicated and imaginary values can emerge.

A phonon spectrum in 3 dimensions has N modes (N = number of atoms in the unit cell), 3N - 3 of them are optical modes. There are three acoustic modes because for any given direction of propagation, there are two transverse and one longitudinal phonons. A magnon spectrum differs from its phonon counterpart in that each spin in a three dimensional crystal has only one degree of freedom. An ion can shift away from its equilibrium in three distinct directions to create a phonon, while a spin can only decrease its projection along the z-axis in one way to create a magnon. This leaves the magnon spectrum with N total branches, N - 1 of which are optical. In AFM cases, the situation is slightly different. The number of spins per unit cell is doubled, but the two spins are not independent. Each 'up' spin in a unit cell will produce a magnon branch which is degenerate in energy to the branch produced by its corresponding 'down' spin, each with frequencies of opposite sign. This results in 2N total magnons and 2N - 2 optical branches, but only N distinct energies and 1 distinct optical branch.

The quadruply degenerate, non-zero frequency gives the energy of the optical mode of CCTO. As expected, its existence depends on the presence of the 5^{th} neighbor interaction which breaks the three-fold sublattice degeneracy of the system. The experimental value [30] of this optical mode is about 7.3 meV, our model gives only 2.8 meV. While the agreement is not perfect, the order of magnitude is correct and the result is at least in the right ballpark.

6.6.1 "Direct" Exchange

So far the interactions between spin sites in CCTO have been investigated in terms of the superexchange interaction. There are of course other interactions present in a magnetic system. One common interaction is known as the direct exchange interaction and

can be expressed as:

$$H_{direct} = \sum_{<i,j>} -J_{ij}^{F}(\mathbf{S_i} \cdot \mathbf{S_j}) + \frac{1}{4} J_{ij}^{F} n_i n_j \tag{6.24}$$

The first component of this term looks identical to the superexchange interaction, but the exchange constant is preceded by a negative sign, causing the alignment of spins to be the energetically favorable over anti-alignment. This term originates from keeping extra terms in the effective one-band Hamiltonian, Eq. 6.2. As before, the t_{ij} term is retained, along with the on-site Coulomb interaction term, U_{iiii}, but now the U_{ijij} term is also kept. The new term included is:

$$H = -\sum_{<i,j>} U_{ijij} c_{is}^{\dagger} c_{js'}^{\dagger} c_{is'} c_{js} \tag{6.25}$$

Using the relation $\mathbf{S}_i = \frac{1}{2} \sum c_{is}^{\dagger} \vec{\sigma}_{ss'} c_{is'}$ with Pauli matrices, $\vec{\sigma}_{ss'}$, the Heisenberg-like expression (Eq. 6.24) emerges, along with an additional constant term, $\frac{1}{4} J_{ij}^{F} n_i n_j$, which is neglected in this development - its only effect is an overall shift in the energy. The direct-exchange constant is:

$$J_{ij}^{F} = \int d^3\vec{x} d^3\vec{y}\, \phi_i^*(\vec{x}) \phi_i(\vec{y}) \mathbf{v}(\vec{x},\vec{y}) \phi_j^*(\vec{x}) \phi_j(\vec{y}) \tag{6.26}$$

The interatomic direct exchange term is often neglected because the orbitals $\{\phi_i\}$ are usually assumed to be atomic orbitals which are so short-ranged that the direct exchange constant, J_{ij}^{F}, is essentially zero. Though Wannier orbitals are localized (as compared to Bloch states), they can be much more extended than atomic orbitals and their direct exchange with neighboring sites cannot be assumed to be negligible.

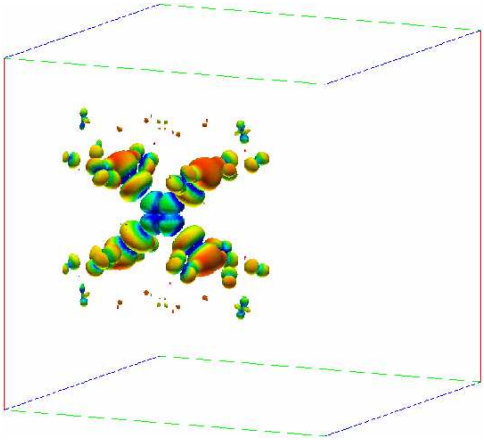

Figure 6.10: One of the three Wannier functions (corresponding to the three magnetic bands) calculated for CCTO. The Kohn-Sham (Bloch) wavefunctions were used to construct the Wannier function by summing over k-points.

The name direct-exchange is so closely associated with these presumed atomic orbitals that this interaction should possibly be given another name entirely when used in terms of Wannier orbitals. Nonetheless, throughout this manuscript, direct exchange will be used to describe the interactions described by Eqs. 6.24, 6.25, 6.26 .

Combining the Heisenberg term which results from 2^{nd} order perturbation theory (superexchange interaction) and the new direct exchange term results in a Hamiltonian which still contains only spin-spin interactions:

$$H = \sum_{<i,j>} (J^{S.E.} - J_{ij}^{F})(\mathbf{S_i} \cdot \mathbf{S_j}) \tag{6.27}$$

If the Wannier orbitals are known, then the t_{ij}'s and J_{ij}^{F}'s can be calculated exactly [39] (see Fig. 6.10 for a picture of a calculated Wannier function) as well as the bare U, which was formerly set by using an educated guess. U is simply the 'on-site' J given by $< ii|V_{ee}|ii >$ (with positive sign). One ambiguity remains, however, and this is due to the inability to exactly deal with the screening of the electron-electron interactions. Since it is the bare

Coulomb interaction term which is included in the Hamiltonian used to calculate the J^F and U matrix elements, the values are certainly too large (nowhere is the 'double-counting' v^{eff} subtracted off), but in exactly what way they are too large is entirely unclear. Though it is the crudest possible correction, dividing these terms by a constant can at least account for the reduction due to screening at a very basic level. There is no reason to suspect that the screening of the hopping terms should be identical to that of the direct exchange terms and in fact, the screening of the U is almost certainly greater than that of J. The exact factors used to reduce the calculated quantities will, in the end, be determined by the necessity of obtaining a physical solution - an AFM ground state with real frequency eigenvalues in the case of CCTO. As a starting point, the calculated bare U (7.59 eV) will be divided by 2.5, as will the bare J^F. The results are tabulated in Table 6.3.

Table 6.3: Calculated superexchange constants and direct exchange constants

# nearest neighbor	$J^{S.E.}$ (meV)	J^F (meV)	$J^{eff} = J^{S.E.}$ - J^F(meV)
1st	0	2.62	-2.62
2nd	0	2.13	-2.13
3rd	3.71	2.49	1.22
4th π(Ca)	4.12	1.18	2.94
4th' π(no Ca)	0.41	0.37	0.04
4th" δ	0.21	0.24	-0.04
5th	0.04	0.14	-0.10
6th	0.01	0.05	-0.04
7th σ	0.0	.08	-0.08
7th' δ (Ca)	0.01	.04	-0.03
7th" δ (no Ca)	0.13	.064	.07

There is no symmetry principle to prohibit direct exchange interactions between 1^{st} and 2^{nd} Cu neighbors (or any neighbors), so J_1^F and J_2^F will be non-zero and should be taken into account in the spin wave Hamiltonian. The terms in the spin Hamiltonian

involving these two neighbors are:

$$H_1 = J_1 sz_1[\sum_{\vec{k}} \gamma_{\vec{k}AB}(\mathbf{Aa}_{\vec{k}}\mathbf{Bb}_{\vec{k}} + \mathbf{Aa}^{\dagger}_{\vec{k}}\mathbf{Bb}^{\dagger}_{\vec{k}} + \mathbf{Ab}_{\vec{k}}\mathbf{Ba}_{\vec{k}} + \mathbf{Ab}^{\dagger}_{\vec{k}}\mathbf{Ba}^{\dagger}_{\vec{k}})$$
$$+ \gamma_{\vec{k}AC}(\mathbf{Aa}_{\vec{k}}\mathbf{Cb}_{\vec{k}} + \mathbf{Aa}^{\dagger}_{\vec{k}}\mathbf{Cb}^{\dagger}_{\vec{k}}vv + \mathbf{Ab}_{\vec{k}}\mathbf{Ca}_{\vec{k}} + \mathbf{Ab}^{\dagger}_{\vec{k}}\mathbf{Ba}^{\dagger}_{\vec{k}}$$
$$+ \gamma_{\vec{k}BC}(\mathbf{Ba}_{\vec{k}}\mathbf{Cb}_{\vec{k}} + \mathbf{Ba}^{\dagger}_{\vec{k}}\mathbf{Cb}^{\dagger}_{\vec{k}} + \mathbf{Bb}_{\vec{k}}\mathbf{Ca}_{\vec{k}} + \mathbf{Bb}^{\dagger}_{\vec{k}}\mathbf{Ca}^{\dagger}_{\vec{k}})$$
$$- 2(\mathbf{Aa}^{\dagger}_{\vec{k}}\mathbf{Aa}_{\vec{k}} + \mathbf{Ba}^{\dagger}_{\vec{k}}\mathbf{Ba}_{\vec{k}} + \mathbf{Ca}^{\dagger}_{\vec{k}}\mathbf{Ca}_{\vec{k}} + \mathbf{Ab}^{\dagger}_{\vec{k}}\mathbf{Ab}_{\vec{k}} + \mathbf{Bb}^{\dagger}_{\vec{k}}\mathbf{Bb}_{\vec{k}} + \mathbf{Cb}^{\dagger}_{\vec{k}}\mathbf{Cb}_{\vec{k}}) \tag{6.28}$$

$$H_2 = J_2 sz_2[\sum_{\vec{k}} \gamma_{\vec{k}AB}(\mathbf{Aa}_{\vec{k}}\mathbf{Ba}^{\dagger}_{\vec{k}} + +\mathbf{Aa}^{\dagger}_{\vec{k}}\mathbf{Ba}_{\vec{k}} + \mathbf{Ab}_{\vec{k}}\mathbf{Bb}^{\dagger}_{\vec{k}} + \mathbf{Ab}^{\dagger}_{\vec{k}}\mathbf{Bb}_{\vec{k}})$$
$$+ \gamma_{\vec{k}AC}(\mathbf{Aa}_{\vec{k}}\mathbf{Ca}^{\dagger}_{\vec{k}} + \mathbf{Aa}^{\dagger}_{\vec{k}}\mathbf{Ca}_{\vec{k}} + \mathbf{Ab}_{\vec{k}}\mathbf{Cb}_{\vec{k}\dagger} + \mathbf{Ab}^{\dagger}_{\vec{k}}\mathbf{Bb}_{\vec{k}}$$
$$+ \gamma_{\vec{k}BC}(\mathbf{Ba}_{\vec{k}}\mathbf{Ca}^{\dagger}_{\vec{k}} + \mathbf{Ba}^{\dagger}_{\vec{k}}\mathbf{Ca}_{\vec{k}} + \mathbf{Bb}_{\vec{k}}\mathbf{Cb}^{\dagger}_{\vec{k}} + \mathbf{Bb}^{\dagger}_{\vec{k}}\mathbf{Cb}_{\vec{k}})$$
$$- 2(\mathbf{Aa}^{\dagger}_{\vec{k}}\mathbf{Aa}_{\vec{k}} + \mathbf{Ba}^{\dagger}_{\vec{k}}\mathbf{Ba}_{\vec{k}} + \mathbf{Ca}^{\dagger}_{\vec{k}}\mathbf{Ca}_{\vec{k}} + \mathbf{Ab}^{\dagger}_{\vec{k}}\mathbf{Ab}_{\vec{k}} + \mathbf{Bb}^{\dagger}_{\vec{k}}\mathbf{Bb}_{\vec{k}} + \mathbf{Cb}^{\dagger}_{\vec{k}}\mathbf{Cb}_{\vec{k}}) \tag{6.29}$$

Like the 5^{th} Cu neighbor interaction, these terms contain complicated combinations of magnon operators, but as before, the same set of 6 operators mix into each other under commutation, and the same diagonalization method may be used. The matrix now gains non-zero terms in all off-diagonal elements, though it retains the same overall symmetry. Since both J_1 and J_2 connect spins in all three sub-lattices, optical magnons can now exist even without the inclusion of the 5^{th} neighbor coupling.

The inclusion of the new terms substantially complicates the overall picture of magnetic interactions and the likelihood of the appearance of imaginary frequencies (unstable antiferromagnetic order) is increased. For neighbors 3^{rd} and higher, there is competition

between the superexchange and direct exchange interactions, but for 1^{st} and 2^{nd} neighbors, no superexchange interaction exists, so the tendency is always for these spins to align. For the 2^{nd} Cu neighbors, this reinforces the overall AFM order of the crystal, whereas for the 1^{st} Cu neighbors, this is a frustrating interaction. The result of adding direct exchange J's to the spin wave Hamiltonian is a competition between the 1^{st} and 3^{rd} nearest Cu neighbor interactions. If J_3^{eff} (= $J_3^{S.E.}$ - J_3^F) dominates, then the proper AFM order results, but if J_1 dominates, the crystal will order ferromagnetically.

The specific process by which this competition arises is somewhat complex. The 2^{nd} neighbor interaction is strictly FM and aligns all 2^{nd} neighbors. A careful inspection of the crystal shows that even 2^{nd} neighbors don't fully connect the whole lattice and therefore the relationship of adjacent spins remains undetermined. Adding the 3^{rd} nearest neighbor interaction fully determines the order of the spins by eliminating the ambiguity in adjacent spins. Given that $J_3^{S.E.} > J_3^F$, which it certainly is, the collusion of these two interactions produces the correct magnetic order. However, the J_1 interaction is disruptive (frustrating) to this order as it tries to align the same nearest neighbor spins which the combination of J_3^{eff} and J_2^F would have anti-aligned. The proper order results only if J_3^{eff} is large enough to overwhelm the effects of J_1. Given the calculated values for all J's, this can happen only if we correct for the screening of the direct exchange interaction by dividing each J^F by an additional factor of ≈ 2. Any lower screening factor results in imaginary eigenvalues, signaling (incorrect) long-range FM order.

When the minimal necessary screening value is applied to the direct exchange constants, all eigenvalues are real and the acoustic mode disperses linearly away from Γ.

The optical magnon is now due to the J_1 and J_2 direct exchange couplings much more than it is due to the relatively small J_5 superexchange coupling, though this factor still contributes. Because the 1^{st} and 2^{nd} neighbor direct interactions are so much stronger than the 5^{th} neighbor interactions, the value of the optical magnon at the Γ point is significantly increased over the superexchange only value. This brings it very near to the experimental value, though this must be somewhat fortuitous as there is no good justification for the screening factor. The entire spin wave spectrum is greatly affected by the inclusion of the direct exchange terms and the effect of J_5, on which the AFM ground state hinged in the superexchange picture, is entirely overwhelmed by the J_1 and J_2 effects.

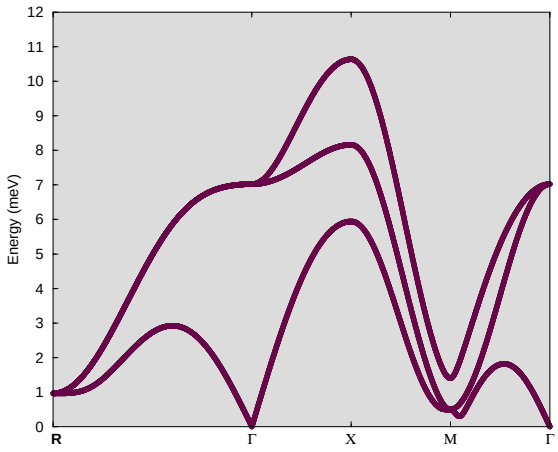

Figure 6.11: The magnon spectrum of CCTO with both superexchange and direct exchange constants included. Since the direct exchange constants which connect all sublattices to one another are much greater than the J_5^{SE} parameter which alone splits the bands in the superexchange picture, the non-degeneracies are very obvious and the shape of the branches is quite distorted from those in Fig. 6.9.

In principle, there is no upper bound for the value of the screening which can be applied to the direct exchange constants. As the value of the screening is increased, the spin wave spectrum gradually returns to its superexchange form. As before, the matrix is

analytically diagonalizable at the Γ point, the acoustic mode is doubly degenerate and the optical modes quadruply degenerate:

$$\epsilon_0 = 0$$

$$\epsilon_0 = \pm\sqrt{3}\sqrt{J_1^2 - 4J_1J_2 + 3J_2^2 + 2J_1J_3 - 2J_2J_3 + 2J_1J_5 - 4J_2J_5 + 2J_3J_5 + J_5^2}$$

With the inclusion of the interactions of 1^{st} and 2^{nd} nearest neighbors, the optical modes exist even without the 5^{th} neighbor coupling. The value of these modes is raised considerably at the Γ point and now very reasonably reproduces the experimental value of $\sim$ 7.34 eV. Because the screening is not taken into account in any rigorous way, the agreement is somewhat artificial. However, the screening could not be any *less* than the value used and still preserve the AFM ground state, and greater screening would bring the experimental and calculated values for the optical phonon even closer.

Chapter 7

EuN

7.1 Introduction

EuN is an insulator with a simple rocksalt structure. The trivalent Eu ion has an f^6 configuration, which through the use of Hund's rules (valid here for the localized f states), yields an overall non-magnetic atomic configuration: $|\vec{J}| = |\vec{L}$ - $\vec{S}| = 3$ - $3 = 0$. The $J = 0$ state does not couple to an external magnetic field, so that the magnetic moment which is non-zero ($\vec{M} = 2\ \vec{S} + \vec{L} = 3$) is equally likely to point in any direction. Though dipolar coupling proceeds through J - J interaction, exchange coupling is a spin interaction. At each site, there is a very large spin moment which could conceivably interact through conventional spin exchange mechanisms, causing the spin moments to order. Alignment (or anti-alignment) of spin moments would necessarily be accompanied by the oppositely ordered orbital moments at each site, since spin-orbit coupling will be strong for the Eu f-states. This ordering would be undetectable to any thermodynamic measurements, but could be observed using neutron scattering which is sensitive to the slightly different struc-

ture factors of the two kinds of moments. Thus, this $J = 0$, "spherical ion" material, may have an underlying order, invisible to most measurements, but perhaps existing even at reasonable temperatures.

7.2 Calculational Methods

It is unclear from the outset whether any order between moments would be AFM or FM, since both direct and superexchange mechanisms seem possible. Therefore, the unit cell is doubled to allow for the possibility of AFM ordering. Many transition metal oxides which share the rocksalt structure of EuN have an AFM ground state in which all second nearest neighbors are anti-aligned. This results in the magnetic structure known as AFMII in which (1,1,1) planes contain all aligned spins and spin direction alternates between adjacent planes.

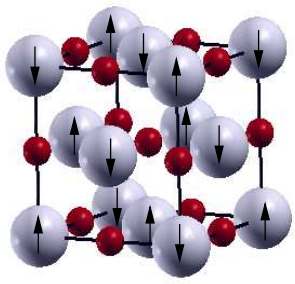

Figure 7.1: The spin ordering of an AFMII compound. All second nearest neighbor spins are anti-aligned

In many rare-earth systems, it is necessary to use the LDA+U method in order to move partially filled states away from the Fermi energy and to obtain the correct insulating solutions. A value of 10 eV has been chosen for the screened Coulomb interaction (U)

and a value of 1 eV for the screened exchange interaction (J) on the Eu ion. These values were chosen by comparison with other Eu compounds, not by direct calculation. The exact values of U and J should not substantially change the conclusions about magnetic ordering which are drawn here, although some Eu compounds of this structure have magnetic phases which depend on U. The value of J is certainly reasonable and the effects of changing it are small, provided it is non-zero. The effect of J on the electronic structure will be discussed in a later section.

All band structure calculations were performed using the program Wien2k [40], which employs an APW+lo basis set. This allows for a lower plane wave cutoff and consequently the RKmax was set to 7.00. The standard LSDA functional to which the U term is added was formulated with the LDA parametrization of Perdew and Wang [32]. The experimental lattice constant [41] of 5.026 $\AA$ was used and all compressions are stated in terms of this value. The RMT values were set to 2.1 a.u. for Eu and 1.8 a.u. for N, which resulted in virtually no core charge leakage at all. For the AFM calculation of EuN, the Wien2k program was temporarily altered to enforce the antiferromagnetic spin symmetry and the corresponding orbital symmetry in the density matrix.

7.3 Electronic Structure

The LDA is extremely insufficient for the localized f states of EuN. The correlation is underestimated so badly that the resulting ground state is metallic and the partially filled f-orbitals straddle the Fermi energy. In reality, the occupied states should be much lower in energy, and an insulating gap is essential in order to study the physics of this compound.

Spin-orbit effects are also important because Eu is a very heavy ion and the f-electrons are fairly tightly bound. Adding an extra correlation term by using the LDA+U procedure allows for the proper orbital polarization which moves 6 majority states completely beneath the Fermi energy, while the final majority state is well above it, along with all 7 minority states. In Fig. 7.2, a comparison of LDA and LDA+U results for the cubic EuN are shown.

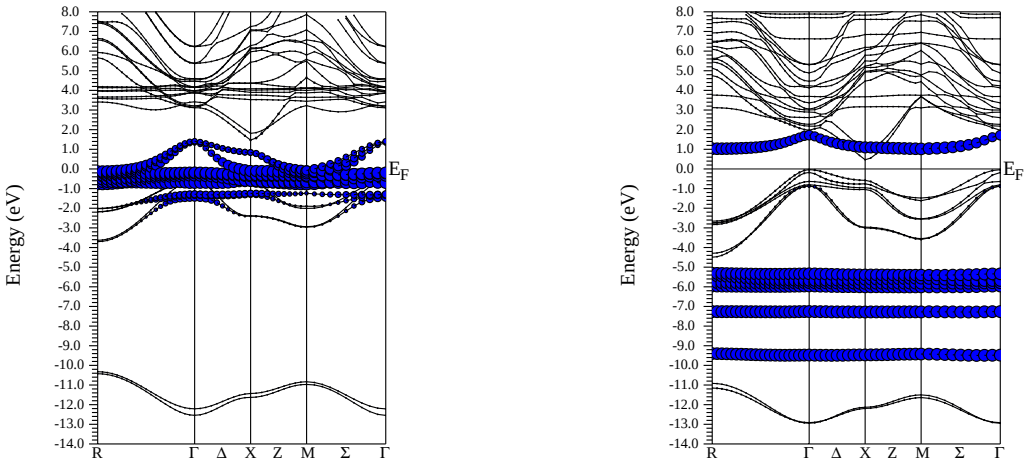

Figure 7.2: Band structures of EuN in the simple unit cell; the f-bands are highlighted *left panel* The erroneous metallic solution given by LDA. *right panel* The LDA+U solution has 6 filled and 1 empty majority spin bands, separated by the value of U

To obtain an AFM solution, it was necessary to first force the proper wave function symmetry. Left to converge freely, the AFM ground state solution will not be found. This is often the case in calculations where the unit cell has been doubled causing the two magnetic ions to be treated independently. Since the wave functions of the two Eu ions in the rhombohedral cell are not truly independent, it suffices to calculate one and specify its symmetry relationship to the other. The anti-alignment of spins takes place in the

f-orbitals to which an additional correlation potential has been added. Therefore, it is necessary to enforce the proper symmetry on the density matrices of the two Eu ions as well. To ensure that the resulting ground state is not artificial, the constraints are released once the calculation has run to self-consistency and the charge density is well-converged. The system remains in the specified symmetry even without the constraint, indicating an energy minimum and justifying the procedure.

An orbitally resolved density of states plot emphasizes the AFM nature of the calculated ground state. It also shows which bands are near the Fermi energy and which could be involved in magnetic interactions. The Eu-d bands are possibly important in terms of exchange interaction. The f-bands are so localized that they do not overlap even with their nearest N neighbors, making superexchange unlikely. Polarized Eu-d states which are considerably more extended than the f-states could provide a mechanism through which the localized moments on the Eu ions could order with respect to each other.

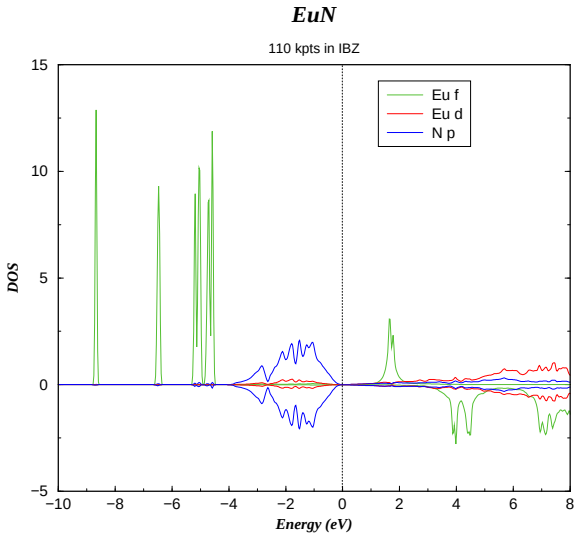

Figure 7.3: A partial and total DOS plot for EuN. The d-bands are less localized than the very peaked f-states

The band structure of the rhombohedral cell is shown in Fig. 7.4. The splitting of the f-bands with respect to one another is not due to a crystal field effect, which should be extremely small for these bands, but rather to differences in the orbitally dependent potential.

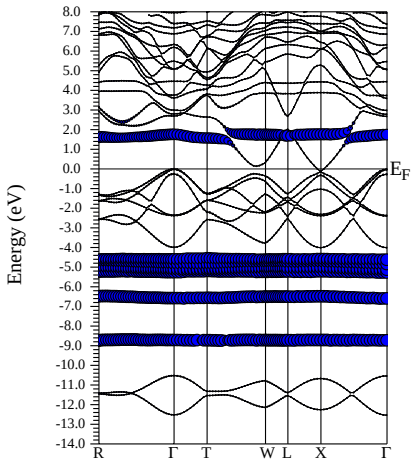

Figure 7.4: The bands of EuN in the doubled, rhombohedral cell. Both up and down plots are identical since the system is AFM and each band is doubly degenerate. The Brillouin zone of the doubled cell is half the size of that of the single cell. Bands at the edges of the single cell BZ have been folded back into the smaller rhombohedral cell so that extra maxima and minima appear as compared to the larger simple cubic BZ of Fig. 7.2

To understand the origin of the splitting between the f-bands, it is necessary to revisit the definition of the correlation matrix elements used in the LDA+U procedure. If the density matrix is diagonal, $n^{\sigma}_{mm'} = n_m \delta_{mm'}$, then the only matrix elements which enter the LDA+U energy are of the form:

$$U_{mm'} =< mm'|V_{ee}|mm' >; \qquad J_{mm'} =< mm'|V_{ee}|m'm > \tag{7.1}$$

If the J input value is set to zero, these simplify to $U_{mm'} = F_0$ and $J_{mm'} = F_0 \delta_{mm'}$. In this case, no distinction between different orbitals is made and filled orbitals will all be shifted downward equally, while unfilled orbitals will be shifted upward equally. Thus, the energy differences based on orbital quantum number (which give rise to Hund's rule splittings in the atomic limit) are absent when J=0. When J is set to a non-zero value, the elements differ depending on the specific orbitals, m and m' entering the integral. Given U and J, the Slater integrals F_0 through F_6 can be calculated and the matrix elements generated [42] using Eq.'s 2.18 and 2.19. Using U = 10eV and J= 1eV, as in the previous calculation, the corresponding Slater integrals are: $F_0 = 10.0$, $F_2 = 11.92$, $F_4 = 7.96$ and $F_6 = 5.89$ and the matrix elements are (ordered from l_z = -3 $\rightarrow$ l_z = 3 from left to right and up to down):

$$U_{mm'} = \begin{bmatrix} 11.391 & 9.842 & 9.239 & 9.056 & 9.239 & 9.842 & 11.391 \\ 9.842 & 10.387 & 9.877 & 9.789 & 9.877 & 10.387 & 9.842 \\ 9.239 & 9.877 & 10.664 & 10.440 & 10.664 & 9.877 & 9.240 \\ 9.056 & 9.789 & 10.440 & 11.431 & 10.440 & 9.789 & 9.056 \\ 9.239 & 9.877 & 10.664 & 10.440 & 10.664 & 9.877 & 9.240 \\ 9.842 & 10.387 & 9.877 & 9.789 & 9.877 & 10.387 & 9.842 \\ 11.391 & 9.842 & 9.239 & 9.056 & 9.239 & 9.842 & 11.391 \end{bmatrix} \quad (7.2)$$

$$J_{mm'} = \begin{bmatrix} 11.391 & 1.550 & 0.947 & 0.528 & 0.475 & 0.370 & 0.740 \\ 1.550 & 10.387 & 1.113 & 1.261 & 0.405 & 0.915 & 0.370 \\ 0.947 & 1.113 & 10.664 & 0.496 & 1.900 & 0.405 & 0.475 \\ 0.528 & 1.261 & 0.496 & 11.431 & 0.496 & 1.261 & 0.528 \\ 0.475 & 0.405 & 1.900 & 0.496 & 10.664 & 1.113 & 0.947 \\ 0.370 & 0.915 & 0.405 & 1.261 & 1.113 & 10.387 & 1.560 \\ 0.740 & 0.370 & 0.475 & 0.528 & 0.947 & 1.550 & 11.391 \end{bmatrix} \quad (7.3)$$

Now the diagonal elements differ from one another and the shifts associated with each orbital are no longer the same. This results in all filled orbitals being shifted downward from the Fermi energy as before, but by an amount which depends on the shape of the orbital. The differences in eigenenergies can be pronounced as in Fig. 7.4 where different f-bands are separated by as much as 2 eV.

7.4 Exchange Energy

The total energies of the AFMII configuration and an FM configuration can be compared by running a calculation in the same doubled, rhombohedral cell, but with the spins all aligned. There is a very small energy difference between the two systems. ΔE = E_{FM} - E_{AFM} = 6.12 meV. This energy difference increases with compression. If the lattice parameter is reduced by $\approx$ 2%, ΔE grows to 43.53 meV. Further reduction of the lattice drives the hybridized Eu-d and Ni-p bands across the Fermi energy into a metallic state. Small compression reduces the total energy of both FM and AFM configurations,

indicating that the theoretical equilibrium lattice constant is lower than the reported lattice constant. This "over-binding" is a typical result of applying the LDA which underestimates electron-electron interactions.

For the purposes of obtaining a value for the exchange constant, J, of the system, the superexchange process in which Eu spins interact through the orbitals of the N ion is assumed to be absent and spin-spin alignment (or anti-alignment) is presumed to take place via nearest neighbor interactions (possibly due to overlapping Eu-d orbitals). In the nearest-neighbor picture, each Eu spin is surrounded by an equal number (six) of up and down spins in the AFM configuration, and by twelve similarly aligned spins in the FM configuration. Using a simple, classical Heisenberg model, the energy difference between these two different magnetic states can be calculated:

$$E_{AFM} = 0, \qquad E_{FM} = JzS^2; \qquad \Delta E = 12JS^2 \tag{7.4}$$

Setting the model and first principles energy differences equal to one another and solving for J yields an energy of .057 meV which corresponds to a temperature of 6.6 K. When the compound is compressed, the interactions become stronger and the value of the exchange parameter increases to .405 meV, or a temperature of 46.94 K. The magnetism of EuN is obviously quite sensitive to pressure and even a moderate amount of compression should raise the Néel temperature considerably.

7.5 A Model Calculation

To investigate the competition or cooperation of different interactions in the EuN system, a simple two-site Hamiltonian was constructed:

$$H = K \sum_{<i,j>} \mathbf{S}_i \cdot \mathbf{S}_j + \lambda \sum_i \mathbf{L}_i \cdot \mathbf{S}_i + \sum_i \mathbf{B} \cdot \mathbf{M} + \sum_i (\mathbf{D} \cdot \mathbf{L})^2 \tag{7.5}$$

The Hamiltonian includes all the interactions thought to be important in the investigation of magnetic ordering in EuN. The various parameters are set using a variety of techniques. The value of λ which sets the energy scale for the spin-orbit interaction was taken from the splitting between J=0 and J=1 levels in other Eu^{3+} compounds [43] and has a value of 340 cm^{-1} = 40 meV. The exchange parameter K (used instead of the traditional 'J' to avoid confusion with the designation for total angular momentum) is taken from calculation on other Eu rocksalt compounds which have different valencies and are magnetic - its value is set to 5 meV. The crystal anisotropy is set to what is considered a reasonable value, 5 meV. The magnetic field B can be varied both in magnitude and direction and is generally taken to be in the z-direction.

The basis set used for this model includes both the J=0 state as well as the J=1 multiplet on each of the two sites. In a purely atomic system, Hund's rules give the J=0 state as the ground state, but if there is more than one site, as in this model, the interactions between spins on different sites or between the orbitals and the lattice (crystal anisotropy)

can mix in the higher multiplet states. This basis gives four different states per site, so the Hamiltonian matrix will be 16 x 16.

In order to calculate the matrix elements, the $|J, J_z>$ states need to be projected onto a set of $|L, L_z; S, S_z>$ states. This can be accomplished using the Clebsch-Gordan coefficients. For every state, the values $|L| = 3$, $|S| = 3$, are used and are therefore left out of the notation. The states are indicated simply by the z components of orbital and spin angular momentum respectively: $|L_z, S_z>$.

$$|J=0, J_z=0> = \frac{1}{\sqrt{7}} \; |-3,3> - \frac{1}{\sqrt{7}}|-2,2> + \frac{1}{\sqrt{7}} \; |-1,1> - \frac{1}{\sqrt{7}}|0,0> + \frac{1}{\sqrt{7}} \; |1,-1> - \frac{1}{\sqrt{7}}|-2,2> + \frac{1}{\sqrt{7}} \; |-3,3> \tag{7.6}$$

$$\begin{aligned} |J=1, J_z=-1> = \; & \frac{\sqrt{3}}{2\sqrt{7}}|2,-3> - \frac{\sqrt{5}}{2\sqrt{7}}|1,-2> + \frac{\sqrt{3}}{\sqrt{14}}|0,-1> - \\ & \frac{\sqrt{3}}{\sqrt{14}}|-1,0> + \frac{\sqrt{5}}{2\sqrt{7}}|2,-1> - \frac{\sqrt{3}}{2\sqrt{7}}|3,-2> \end{aligned}$$

$$\begin{aligned} |J=1, J_z=0> = - \; & \frac{3}{2\sqrt{7}}|-3,3> + \frac{1}{\sqrt{7}}|-2,2> - \frac{1}{2\sqrt{7}}|-1,1> + \\ & \frac{1}{2\sqrt{7}}|1,-1> - \frac{1}{\sqrt{7}}|-2,2> + \frac{3}{2\sqrt{7}}|-3,3> \end{aligned} \tag{7.7}$$

$$\begin{aligned} |J=1, J_z=1> = \; & \frac{\sqrt{3}}{2\sqrt{7}}|3,-2> - \frac{\sqrt{5}}{2\sqrt{7}}|2,-1> + \frac{\sqrt{3}}{\sqrt{14}}|1,0> - \\ & \frac{\sqrt{3}}{\sqrt{14}}|0,1> + \frac{\sqrt{5}}{2\sqrt{7}}|-1,2> - \frac{\sqrt{3}}{2\sqrt{7}}|-2,3> \end{aligned}$$

(7.8)

With the basis states now in terms of eigenstates of the **L** and **S** operators, the Hamiltonian matrix can be constructed and diagonalized numerically. Different expectation values (correlation functions) can also be calculated in order to investigate the onset of

ordering.

With K, B, and D set to zero, the system behaves like two isolated atoms - the $|J = 0, J_z = 0 >$ basis state is the ground state eigenstate of each site. In the very limited Hilbert space of the ground state $< L_z >$, $< S_z >$, and $< M_z >$ are all zero and there is no relationship between the two sites at all.

If only the Heisenberg term is kept and all others are set to zero, none of the basis states are eigenstates. If the K is positive, individual spin-rotation symmetry is broken,the spins anti-align, and the calculated value of $< S_1 \cdot S_2 >$ = -7.18. This value can also be calculated analytically, using the same values for $|S|$ and $|L|$ as before:

$$\begin{aligned} \mathbf{S}_1 \cdot \mathbf{S}_2 &= \frac{(S_{Tot}^2 - S_1^2 - S_2^2)}{2} \\ &= \frac{0^2 - 3(3+1) - 3(3+1)}{2} = -12 \end{aligned} \tag{7.9}$$

Since $0 \leq |S_{Tot}| \leq 6$, the lowest energy state occurs for $|S_{Tot}| = 0$. The reason the analytic and calculated values differ is that the basis states chosen for our model do not span the entire Hilbert space of the Heisenberg Hamiltonian. In order to obtain the full anti-alignment of the analytic solution, higher J multiplets would have to be included in the basis. If the Heisenberg term were the only interaction, these states would be necessary. But the spin-orbit constant, λ, sets the energy scale of the problem and this interaction moves the higher J multiplets too high in energy to be considered. Therefore, an expectation value, $< \mathbf{S}_1 \cdot \mathbf{S}_2 >$ = -7.18 will be considered maximum anti-alignment for this model.

If all interaction terms in the model are kept, but the external magnetic field, $\mathbf{B}$ is set to zero, the alignment of the spins as a function of the Heisenberg parameter can be

plotted as in Fig. 7.5 When λ is infinite (or K is zero), the spin-orbit interaction defines the ground state ($|J = 0, J_z = 0 >$) and there is no alignment. As the Heisenberg parameter grows, the spins become more and more anti-aligned. The value of the dot product of spins asymptotes toward the maximum of -7.18.

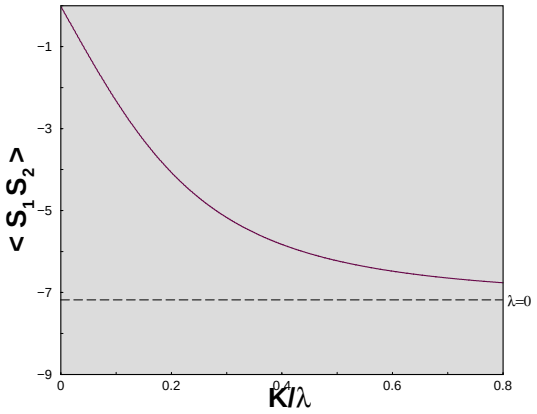

Figure 7.5: Alignment of spins as a function of K/λ. The horizontal line is the maximum alignment possible in the restricted Hilbert space of the model

For small K, the order parameter grows linearly with K. Once the ratio K/λ has grown to 0.175, the correlation function has already reached half its maximum value. Because the curve is initially so steep, modest values of the exchange parameter are sufficient to produce negative spin-spin correlation.

Plotting the expectation value of the anti-alignment of moments, $< \mathbf{M}_1 \cdot \mathbf{M}_2 >$, yields a very similar result. As before, the Hilbert space is too small to include full anti-alignment of moments:

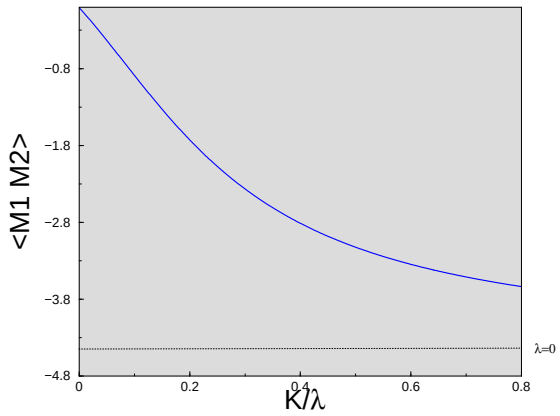

Figure 7.6: Alignment of moments as the value of the exchange parameter varies. The maximal anti-alignment is plotted as a horizontal line

For both spins and magnetic moments, as λ goes to infinity, the ground state collapses into the J=0 state, no alignment is possible. Neither the spin magnitude nor the magnetic moment magnitude is zero, but there is no preferred direction of orientation overall and the moment (and spin) at each site spends an equal amount of time pointing each way, resulting in no overall alignment. The spin-spin interaction and the crystal anisotropy both move the system out of the J=0 state, mixing in the J=1 multiplet. Once the ground state Hilbert space is expanded by this mixing, alignment is possible and occurs due to the Heisenberg term which makes it energetically favorable. The expectation value of the magnetic moment in any given direction is likely still very close to zero, but the spins now have interactions with each other and point in opposite directions, and a non-zero order parameter develops.

The first principles calculation suggests that a non-zero spin-spin interaction does indeed exist. Though the energy difference between spin orientations is rather small, it is certainly non-zero and can be increased with pressure. The model calculation shows that,

at least in a two site system, any non-zero interaction expands the Hilbert space and results in alignment or anti-alignment of the spins. Though the model was carried out assuming that K was positive, the total energy calculation points to a negative exchange constant.

There are other Eu rocksalt compounds with FM ordering, as well as those with AFM ordering. In some cases, such as EuSe, a transition between the two magnetic configurations can be driven by manipulating the U parameter [44] or by applying pressure. A state in which the spin moments of Eu ions are anti-ferromagnetically ordered seems unlikely for EuN, but a hidden ferromagnetic arrangement of spins (accompanied by an identical, but oppositely pointed arrangement of orbital moments) is both possible and energetically favorable.

Bibliography

[1] H. Hohenberg and W. Kohn, Phys. Rev. **136**, B864 (1964).

[2] W. Kohn and L. J. Sham, Phys. Rev. **140**, A1133 (1965).

[3] J. C. Slater, *The Self-Consistent Field for Molecules and Solids* (McGraw-Hill, New York, ADDRESS, 1974).

[4] O. K. Andersen, Solid State Commun. **13**, 133 (1973).

[5] D. J. Singh, Phys. Rev. B **41**, 6388 (1991).

[6] E. Sjostedt, L. Nordstrom, and D. J. Singh, Solid State Comm. **114**, 15 (2000).

[7] V. I. Anisimov, J. Zaanen, and O. K. Andersen, Phys. Rev. B **44**, 943 (1991).

[8] A. B. Shick, A. I. Lichtenstein, and W. E. Pickett, Phys. Rev. B **60**, 10763 (1999).

[9] F. M. F. De Groot, J. C. Fuggle, B. T. Thole, and G. A. Sawatzky, Phys. Rev. B **42**, 5459 (1990).

[10] V. I. Anisimov, I. V. Solovyev, M. A. Korotin, M. T. Czyzyk, and G. A. Sawatzky, Phys. Rev. B **48**, 16929 (1993).

[11] P. H. Dederichs, S. Blugel, R. Zeller, and H. Akai, Phys. Rev. Lett. **53**, 2512 (1984).

[12] V. I. Anisimov and O. Gunnarsson, Phys. Rev. B **43**, 7570 (1991).

[13] M. T. Czyzyk and G. A. Sawatzky, Phys. Rev. B **49**, 14211 (1994).

[14] A. G. Petukhov, I. I. Mazin, L. Chioncel, and A. I. Lichtenstein, Phys. Rev. B **67**, 153106 (2003).

[15] N. W. Ashcroft and N. D. Mermin, *Solid State Physics* (Saunders College, ADDRESS, 1976).

[16] S. S. Saxena, P. Agarwal, K. Ahilan, F. M. Grosche, R. K. Haselwimmer, M. J. Steiner, E. Pugh, I. R. Walker, S. R. Julian, P. Monthoux, G. G. Lonzarich, A. Huxley, I. I. Sheikin, and D. Braithwaite, Nature **406**, 587 (2000).

[17] A. Huxley, I. Sheikin, E. Ressouche, N. Kernavanois, D. Braithwaite, R. Calemczuk, and J. Flouquet, Phys. Rev. B **63**, 144519 (2001).

[18] T. He, Q. Huang, A. P. Ramirez, Y. Wang, K. A. Regan, N. Rogado, M. A. Hayward, M. K. Haas, J. S. Slusky, K. Inumara, H. W. Zandbergen, N. P. Ong, and R. J. Cava, Nature **411**, 54 (2001).

[19] P. Blaha, K. Schwarz, and J. Luitz, 1999, wien97, A full Potential Linearized Augmented Plane Wave Package for Calculating Crystal Properties.

[20] J. P. Perdew, K. Burke, and M. Ernzerhof, Phys. Rev. Lett. **77**, 3865 (1996).

[21] O. Gunnarsson, J. Phys. F **6**, (1976).

[22] P. M. Marcus and V. L. Moruzzi, Phys. Rev. B **38**, 6949 (1988).

[23] D. M. Teter, G. V. Gibbs, M. B. Boisen, D. C. Allan, and M. P. Teter, Phys. Rev. B **52**, 8064 (1995).

[24] A. P. Ramirez, M. A. Subramanian, M. Gardel, G. Blumberg, D. Li, T. Vogt, and S. M. Shapiro, Solid State Comm. **115**, 217 (2000).

[25] C. C. Homes, T. Vogt, S. M. Shapiro, S. Wakimoto, M. A. Subramanian, and A. P. Ramirez, Phys. Rev. B **67**, 092106 (2003).

[26] M. A. Subramanian, D. Li, N. Duan, B. A. Reisner, and A. W. Sleight, J. Solid State Chem. **151**, 323 (2000).

[27] C. Lacroix, J. Phys. C: Solid St. Phys. **13**, 5125 (1980).

[28] A. Collomb, D. Samaras, B. Bochu, and J. C. Joubert, Phys. Stat. Sol. (a) **41**, 459 (1977).

[29] A. Koitzsch, G. Blumberg, A. Gozar, B. Dennis, A. P. Ramirez, S. Trebst, and Shuichi Wakimoto, Phys. Rev. B **65**, 052406 (2002).

[30] Y. J. Kim, S. Wakimoto, S. M. Shapiro, P. M. Gehring, and A. P. Ramirez, Solid State Comm. **121**, 625 (2002).

[31] B. Bochu, M. N. Deschizeaux, and J. C. Joubert, J. Solid State Chem **29**, 291 (1979).

[32] J. P. Perdew and Y. Wang, Phys. Rev. B. **45**, 13244 (1992).

[33] L. He, J. B. Neaton, M. H. Cohen, D. Vanderbilt, and C. C. Homes, Phys. Rev. B **65**, 214112 (2002).

[34] H. Rosner, "Electronic Structure and Exchange Integrals of Low Dimensional Cuprates", Doctoral Dissertation.

[35] D. Papaconstantopoulos, *Handbook of the BAnd Structure of Elemental Solids* (Plenum Pub Corp, ADDRESS, 1986).

[36] J. C. Slater and G. F. Koster, Phys. Rev. **94**, 844 (1954).

[37] T. H. H. Primakoff, Phys. Rev. **58**, 1908 (1940).

[38] N. Bogoliubov, J. Phys. Moscow **11**, 23 (1947).

[39] W. Ku.

[40] P. Blaha, K. Schwarz, G. K. H. Madsen, D. Kvasnicka, and J. Luitz, WIEN2K, 2002, an Augmented Plane Wave + Local Orbitals Program for Calculating Crysteal Properties (Karlheinz Schwarz, Techn. Universitat Wien, Austria), ISBN 3-9501031-1-2.

[41] J. Kordis and K. A. Gingerich, J. Am. Ceramic Soc. **56**, 581 (1973).

[42] A. Shick, the calculation of Slater integrals and matrices was done with the program of Sasha Shick.

[43] Tezuka and Hinatsu, J. Solid State Chem. **138**, 342 (1998).

[44] J. Kunes, Unpublished .